Fully explicit numerical scheme for linearized wave propagation in nearly-incompressible soft hyperelastic solids

Giulia Merlini, Sébastien Imperiale, Jean-Marc Allain

Fully explicit numerical scheme for linearized wave propagation in nearly-incompressible soft hyperelastic solids

Giulia Merlini[1,2], **Jean-Marc Allain**[1,2], **Sebastien Imperiale**[2,1]

[1]LMS, Ecole Polytechnique, CNRS – Institut Polytechnique de Paris; [2]Inria, Team-MΞDISIM, Inria-Saclay Ile de France 91120 Palaiseau

✉ **For correspondence:** sebastien.imperiale@inria.fr

Abstract

The numerical approximation of wave propagation problems in nearly or pure incompressible solids faces several challenges such as locking and stability constraints. In this work we propose a stabilized Leapfrog scheme based on the use of Chebyshev polynomials to relax the stability condition, which is strongly limited by the enforcement of incompressibility. The scheme is fully explicit, second order accurate and energy-preserving. For the space discretization we use a mixed formulation with high-order spectral elements and mass-lumping. A strategy is proposed for an efficient and accurate computation of the pressure contribution with a new definition of the discrete Grad-div operator. Finally, we consider linear wave propagation problems in nearly-incompressible hyperelastic solids subject to static preload.

Contents

1 Introduction

The accurate and efficient simulation of wave propagation in nearly incompressible solids represents a significant challenge in numerical modeling. Classically, the finite element approximation of solids relies on the displacment-based method, in which it is assumed that the displacement of a body is completely specified by the nodal point displacement [**Sussman1987**]. However, the enforcement of incompressibility highly affects the accuracy of the solution, such that a finer space discretization will be needed, compared to the compressible case. This is due to the fact that volumetric strains are computed with a lower accuracy with respect to the displacements and are close to zero in the incompressible limit. Any error related to the computation of the volumetric strain will result in a large error in the computation of the stress (pressure) due to the multiplication by a large bulk modulus, and then a wrong prediction of the displacement obtained from the principle of virtual work [**Bathe2006**]. With a higher spatial resolution, we may circumvent errors in the computation of the displacement field, but we will still have spurious or incorrect pressure. In addition, it is known [**Sussman1987**, **Oden1970**, **Taylor1968**, **Caforio2018**] that for nearly-incompressible solids, this method suffers from ill-conditioning of the stiffness matrix. In general, we may refer to formulation whose predictive capability is dependent from the bulk modulus as locking formulations [**Bathe2006**, **LeTallec1994**]. Nevertheless, efforts have been done to overcome these limitations, since most of large-scale structural analysis programs are based on displacement-based method [**ELGUEDJ2008**]. We cite in particular the B-scheme for finite-deformation problems [**Hughes1977equivalence**] and F-scheme for hyperelastic problems, which rely on the reduction of volumetric constraints through projection.

Mixed methods form another class of methods for finite element approximations, that have proven to be effective to avoid locking behavior in the framework of elasticity with nearly or pure incompressible materials. These methods are based on the introduction of the pressure as an additional unknown. The problem becomes now a saddle-point problem where the key aspect for the finite-element approximation is the introduction of an auxiliary finite element space for the computation of the pressure field. These methods are proven to be stable under the well-known LBB inf-sup condition derived by Brezzi and Babuska, together with the ellipticity condition

[**Brezzi1974**, **Babuvska1973**, **Boffi2017**], for which the choice of the finite element spaces is fundamental to guarantee stability and convergence of the method. When the stability is not given for a certain choice of the finite element spaces, it is possible to apply stabilization techniques such as cross-grid triangulation or with the introduction of a stabilization in order to relax the incompressibility constraint. We refer the reader to [**Quarteroni2008**] for a review of stabilization methods [**brezzi1984stabilization**] such as Galerkin-Least Square [**HughesFranca**], Streamline Upwind Petrov Galerkin [**hughes1986new**] and bubble functions [**baiocchi1993virtual**].

In addition, the simulation of dynamic problems must account for an appropriate discretization strategy in time. For elastic wave propagation problem is generally prohibitive to use implicit schemes, as they require the inversion of the stiffness matrix at each time-step, which is too large to be stored even when considering factorization methods. Explicit is well suited given the phenomena that we are observing. In particular, the leapfrog (LF) scheme based on centered finite difference of second order time differential equation benefits of several properties: second-order accuracy, energy conservation for linear problems and time reversibility [**hairer2006geometric**]. However, the stability of the scheme is given under the classical CFL condition for the maximal time-step, which is highly constraining when considering nearly incompressibility. As the bulk approaches the incompressible limit, the maximal time-step goes to zero, with resulting endless computations.

A possible alternative is to use fractional step projection methods, in which the idea is to split the original problem in two simpler ones, such that at each time step we compute implicitly a first half-step considering one sub-problem, and then we correct the obtained solution with the second half of the problem that we compute explicitly [**quarteroni2009modellistica**]. We cite in particular [**Caforio2018**], which has been a starting point for this work in order to treat linear elastic wave propagation problems in nearly or pure incompressible solids. The conservative scheme proposed by Caforio et al.[**Caforio2018**] is based on the relaxation of the volumetric component of the displacement solution, related to the incompressible constraint, by solving at each iteration in time a Poisson problem. Then, the explicit leapfrog time-discretization method is used to solve the second part of the problem to account for the "shear" part of the problem. Solving the Poisson problem must then involve the use of fast solvers, like FFT solvers.

In this work, we focus on the development of a fully explicit scheme, such that only the mass matrix will be inverted together with mass-lumping approximation [**Cohen2002**]. Recently, [**Carle2020**] have proposed a new class of methods, named Leapfrog-Chebyshev (LFC) scheme for the relaxation of the CFL condition. They applied Chebyshev polynomials to the linear component of the problem, while the non-linear part is computed with the LF scheme. These schemes have proven to be effective together with local-time stepping methods (LFC-LTS) [**Grote2021**], which are developed to deal with stability constraint related to local mesh refinement. Here, we would like to apply the same idea, but for the incompressibility constraint. We propose, indeed, a novel explicit formulation to treat linear wave propagation in nearly-incompressible problems, such as follows

$$\underline{u}_h^{n+1} - 2\underline{u}_h^n + \underline{u}_h^n + \Delta t^2 M_h^{-1} A_h^s \underline{u}_h^n + \mathscr{R}_{m+1}^{\nu}(\Delta t^2 \lambda M_h^{-1} \bar{A}_h^p)\underline{u}_h^n = \Delta t^2 M_h^{-1} \underline{f}^n$$

where M_h is the lumped mass operator,A_h^s corresponds to the shear-stiffness operator (independent of volumetric parameters), $\bar{A}_h^p$ is a discretized Grad-div operator multiplied by the bulk modulus λ taken positive and very large, and $\mathscr{R}_{m+1}^{\nu}$ is the

damped Chebyshev polynomial of order $m+1$, to be later presented. As explained in [**Carle2020**], it should be interpreted as a multi-rate scheme, such that we evaluate the shear part once, while the volumetric part is iterated as many times as the order $m+1$ of the Chebyshev polynomial. The scheme is stable under the following condition

$$\Delta t^2 \leq \frac{1}{\rho(M_h^{-1}A_h^s)} \qquad \text{and} \qquad m+1 \geq \sqrt{\lambda}\frac{\sqrt{\rho(\Delta t^2 M_h^{-1}\bar{A}_h^p)}e^{\nu/4}}{2}$$

where we denote $\rho(\cdot)$ as the spectral radius of the operator. We underline that the new time-step is now only dependent on the shear operator, while the incompressibility constraint determines the minimum order of the Chebyshev polynomial to guarantee stability.

This method has been developed in the perspective of reproducing elastographic measurements of biological tissues, for the analysis of the material properties and the detection of pathologies. These materials are precisely characterized by a high water content that makes them almost incompressible, and they exhibit hyperelastic (nonlinear) behavior. We must also consider that in a physiological framework, these tissues are generally subjected to certain loading conditions, which then generate a state of pre-stress and pre-deformation of the tissue that affects wave propagation during elastographic measurements. In the following work we have derived a novel formulation for linear wave propagation in nearly incompressible pre-loaded solids, for which we separate the Grad-div operator (volumetric term) from the stiffness operator. The isolation of the term related to the enforcement of incompressibility allows us to tackle the critical aspects related to accuracy, stability and efficiency that we have mentioned before with the presented Chebyshev Leapfrog scheme.

2 Modelling elastic wave propagation in nearly incompressible non-linear solid

In this section we derive the continuous formulation of wave propagation problem in the framework of hyperelastic nearly-incompressible solids. In particular, we consider a small amplitude elastic wave propagating in the solid subjected to a quasi-static load with large deformations. We follow the procedure of linearization as described in [**Destrade2007**, **Shams2011**, **Cafor2019These**, **Dalmora2023**], with the primary aim of presenting the problem and the related notation. The second objective is to derive a weak formulation for linear wave propagation problems in nearly-incompressible preloaded solids, for which the volumetric term is separated from the stiffness operator and is written as a Grad-div operator.

2.1 Kinematics and the non-linear elastodynamic problem

We define $\Omega(t)$ as the domain occupied by a deformable solid at time t. We assume that its boundary $\Gamma(t)$ is sufficiently smooth, such that the outward normal $\underline{n}(t)$ is always defined. For the formulation of the non-linear problem we use a Lagrangian description, which consists in representing the position of points in $\Omega(t)$ with respect to a reference configuration $\widehat{\Omega}$. All the material points in $\widehat{\Omega}$ are described by the coordinate system $\underline{\xi}$ and we can retrieve the *current* (at time t) position of points in $\Omega(t)$ with the bijective deformation map $\underline{\phi}(\underline{\xi},t)$:

$$\underline{\phi} : \underline{\xi} \rightarrow \underline{x}(\underline{\xi},t) = \underline{\phi}(\underline{\xi},t), \qquad \underline{\phi}(\widehat{\Omega}) = \Omega(t)$$

From the definition of the bijective map, we define the *displacement field*

$$\underline{u}(\underline{\xi},t) = \underline{\phi}(\underline{\xi},t) - \underline{\xi} = \underline{x}(\underline{\xi},t) - \underline{\xi}$$

and the deformation gradient with its determinant

$$\underline{\underline{F}}(\underline{u}(\underline{\xi},t)) = \underline{\underline{\nabla}}_{\xi}\underline{\phi} = \underline{\underline{\mathbb{1}}} + \underline{\underline{\nabla}}_{\xi}\underline{u} \qquad \text{and} \qquad J(\underline{u}) = \det \underline{\underline{F}}(\underline{u})$$

The volume element $\mathrm{d}\Omega$ in the current configuration is then given by the quantity $J(\underline{u})\mathrm{d}\widehat{\Omega}$, while the current area element $\mathrm{d}s$ is equal to $J|\underline{\underline{F}}^{-T}\cdot\underline{n}|\mathrm{d}\hat{s}$. We suggest the reader to look into [**Ciarlet1988**] for details. Before introducing the relevant mechanical quantities to describe the deformation of the solid, we underline that for second order tensors we use the dot-product and double dot-product defined as follows

$$\underline{\underline{A}}\cdot\underline{\underline{B}} = A_{ik}B_{kj}\underline{e}_i\otimes\underline{e}_j, \qquad \underline{\underline{A}}:\underline{\underline{B}} = \mathrm{tr}(A^T\cdot B) = A_{ij}B_{ij}$$

We then introduce the Cauchy-Green deformation tensor $\underline{\underline{C}}(\underline{u}) = \underline{\underline{F}}(\underline{u})^T\cdot\underline{\underline{F}}(\underline{u})$, the Green-Lagrange strain tensor $\underline{\underline{e}}$ and its linearized expression $\underline{\underline{\varepsilon}}$

$$\underline{\underline{e}}(\underline{u}) = \frac{1}{2}(\underline{\underline{C}} - \underline{\underline{\mathbb{1}}}) = \frac{1}{2}(\underline{\underline{\nabla}}_{\xi}\underline{u} + \underline{\underline{\nabla}}_{\xi}\underline{u}^T + \underline{\underline{\nabla}}_{\xi}\underline{u}^T\cdot\underline{\underline{\nabla}}_{\xi}\underline{u}), \qquad \underline{\underline{\varepsilon}}(\underline{u}) = \frac{1}{2}(\underline{\underline{\nabla}}_{\xi}\underline{u} + \underline{\underline{\nabla}}_{\xi}\underline{u}^T)$$

Fundamental law of dynamics

Before presenting the functional spaces in which we will seek the displacement solutions, we define the boundary $\Gamma(t) = \Gamma_D \cup \Gamma_N(t)$, where $\Gamma_N(t)$ is the part of the boundary on which we have a free surface condition, while on the rest of the boundary we consider Dirichlet's condition, meaning that the displcament vanishes. Then, the functional spaces of the displacement field are defined as follows

$$\mathcal{V}(\widehat{\Omega}) := \{\underline{\widehat{v}} \in \mathrm{H}^1(\widehat{\Omega})^d \mid \quad \underline{\widehat{v}} = 0 \text{ on } \Gamma_D\}, \quad \mathcal{V}(\Omega) := \{\underline{v} \in \mathrm{H}^1(\Omega)^d \mid \quad \underline{v} = 0 \text{ on } \Gamma_D\}$$

with dimension $d = 2$ or $d = 3$, and

$$\mathcal{W}(\widehat{\Omega}) \subset \mathcal{V}(\widehat{\Omega}), \quad \mathcal{W}(\Omega) \subset \mathcal{V}(\Omega)$$

with $\mathcal{W}$ as the space of admissible displacements for the non-linear problem, which ensures the existence of the solution. We consider that the solid is subjected to a force $\underline{f}$ per unit mass. Given the observation time T, we write the standard weak formulation associated to the wave propagation problem defined in the current configuration Ω:

For any $t \in [0,T]$, find $\underline{u}(t) \in \mathcal{W}(\Omega)$ such that

$$\int_{\Omega} \varrho(\partial_{tt}\underline{u}\circ\underline{\phi}^{-1} - \underline{f})\cdot\underline{v}\,\mathrm{d}\Omega + \int_{\Omega}\underline{\underline{\sigma}}:\underline{\underline{\nabla}}_{\underline{x}}\underline{v}\,\mathrm{d}\Omega = 0 \qquad \forall\,\underline{v}\in\mathcal{V}(\Omega), \tag{1}$$

where ϱ is the density in the current configuration and $\underline{\underline{\sigma}}$ is the Cauchy stress tensor defined in $\Omega(t)$. In classical continuum mechanics, this problem is named *principle of virtual work* and it is formally equivalent to the *equilibrium equation* with boundary condition of traction in the current configuration $\Omega(t)$. The focus of this work is the description of the wave propagation phenomena in materials with non-linear behavior, namely hyperelastic materials, so that a constitutive law must be introduced to relate internal stress and deformation of the solid due to external loads. Furthermore, we remark that the current configuration in which the problem is written is unknown, so that it is classical to express the problem in a total Lagrangian form with respect to the

reference configuration. We may neglect some details as it is a classical development, for which we refer again the reader to [**Ciarlet1988**].

As a first step towards the Lagrangian form, we remark that for any quantity $\underline{w}(\xi)$ defined in $\widehat{\Omega}$, we have that

$$\int_{\Omega} \underline{w} \circ \underline{\phi}^{-1}(\underline{x}) \, \mathrm{d}\Omega = \int_{\widehat{\Omega}} J \, \underline{w}(\underline{\xi}) \, \mathrm{d}\widehat{\Omega} \tag{2}$$

and the gradient of a field in the reference configuration can be rewritten in the current configuration using

$$(\underline{\underline{\nabla}}_{\xi} \underline{w}) \circ \underline{\phi}^{-1} = \underline{\underline{\nabla}}_{\underline{x}} (\underline{w} \circ \underline{\phi}^{-1}) \cdot (\underline{\underline{F}} \circ \underline{\phi}^{-1}). \tag{3}$$

We rewrite first the inertial term in $\widehat{\Omega}$

$$\int_{\Omega} \varrho (\partial_{tt} \underline{u} \circ \underline{\phi}^{-1} - \underline{f}) \cdot \underline{v} \, \mathrm{d}\Omega = \int_{\widehat{\Omega}} \varrho \circ \underline{\phi}(\underline{\xi}) (\partial_{tt} \underline{u} - \underline{f} \circ \underline{\phi}(\underline{\xi})) \cdot \underline{\widehat{v}} \, J \mathrm{d}\widehat{\Omega} \; = \int_{\widehat{\Omega}} \widehat{\varrho} (\partial_{tt} \underline{u} - \underline{\widehat{f}}) \cdot \underline{\widehat{v}} \, \mathrm{d}\widehat{\Omega}. \tag{4}$$

where we note the mass density in the reference configuration $\widehat{\varrho} : \widehat{\Omega} \to \mathbb{R}$, and is given by $\widehat{\varrho}(\underline{\xi}) = J \varrho \circ \underline{\phi}$. We also define the body force in the reference configuration as $\underline{\widehat{f}} := \underline{f} \circ \underline{\phi}(\underline{\xi})$.

For the stress tensor, we introduce the Second Piola Kirchhoff tensor $\underline{\underline{\Sigma}}$, which corresponds to the symmetric stress tensor defined in the reference configuration, related to the Cauchy stress tensor by the following relation:

$$\underline{\underline{\sigma}} = J^{-1} \underline{\underline{F}} \cdot \underline{\underline{\Sigma}} \cdot \underline{\underline{F}}^{T} \, . \tag{5}$$

We have

$$\int_{\Omega} \underline{\underline{\sigma}} : \underline{\underline{\nabla}}_{\underline{x}} \underline{v} \, \mathrm{d}\Omega = \int_{\widehat{\Omega}} J^{-1} \underline{\underline{F}} \cdot \underline{\underline{\Sigma}} \cdot \underline{\underline{F}}^{T} : \underline{\underline{\nabla}}_{\xi} \underline{\widehat{v}} \cdot \underline{\underline{F}}^{-1} \, J \, \mathrm{d}\widehat{\Omega} = \int_{\widehat{\Omega}} \underline{\underline{\Sigma}} : \underline{\underline{F}}^{T} \cdot \underline{\underline{\nabla}}_{\xi} \underline{\widehat{v}} \, \mathrm{d}\widehat{\Omega} \, .$$

We then introduce the Gateaux derivative of the Green-Lagrange strain tensor $\underline{\underline{e}}$ at $\underline{u}$ in the direction $\underline{\widehat{v}}$ given by the following equation

$$\mathrm{D}\underline{\underline{e}}(\underline{u}) \cdot \underline{\widehat{v}} = \frac{1}{2} \left(\underline{\underline{\nabla}}_{\xi} \underline{\widehat{v}}^{T} \cdot \underline{\underline{F}}(\underline{u}) + \underline{\underline{F}}(\underline{u})^{T} \cdot \underline{\underline{\nabla}}_{\xi} \underline{\widehat{v}} \right) \tag{6}$$

for which we recall the definition of the Gateaux derivative

$$\mathrm{D}A(\underline{u}) \cdot \underline{w} = \lim_{h \to 0} \frac{A(\underline{u} + h\underline{w}) - A(\underline{u})}{h} \, .$$

As $\underline{\underline{\Sigma}}$ is a symmetric tensor, we can consider the contraction with the symmetrized version of $\underline{\underline{F}} \cdot \underline{\underline{\nabla}}_{\xi}$, that corresponds to

$$\int_{\widehat{\Omega}} \underline{\underline{\Sigma}} : \underline{\underline{F}}^{T} \cdot \underline{\underline{\nabla}}_{\xi} \underline{\widehat{v}} \, \mathrm{d}\widehat{\Omega} = \int_{\widehat{\Omega}} \underline{\underline{\Sigma}} : \frac{1}{2} \left(\underline{\underline{F}}^{T} \cdot \underline{\underline{\nabla}}_{\xi} \underline{\widehat{v}} + \underline{\underline{\nabla}}_{\xi} \underline{\widehat{v}}^{T} \cdot \underline{\underline{F}} \right) \mathrm{d}\widehat{\Omega} = \int_{\widehat{\Omega}} \underline{\underline{\Sigma}} : \mathrm{D}\underline{\underline{e}}(\underline{u}) \cdot \underline{\widehat{v}} \, d\widehat{\Omega} \, . \tag{7}$$

Combining (4) and (7) we obtain the *weak formulation in the reference configuration*, that reads:

For any $t \in [0; T]$, find $\underline{u} \in \mathcal{W}$ such that

$$\int_{\widehat{\Omega}} \widehat{\varrho} (\partial_{tt} \underline{u} - \underline{\widehat{f}}) \cdot \underline{\widehat{v}} \, \mathrm{d}\widehat{\Omega} + \int_{\widehat{\Omega}} \underline{\underline{\Sigma}} : \mathrm{D}\underline{\underline{e}}(\underline{u}) \cdot \underline{\widehat{v}} \, d\widehat{\Omega} = \int_{\widehat{\Gamma}_N} \underline{\hat{t}} \cdot \underline{\widehat{v}} \, \mathrm{d}\hat{s} \qquad \forall \, \underline{\widehat{v}} \in \mathcal{V}(\widehat{\Omega}) \tag{8}$$

In the framework of hyperelastic materials, the state of stress within the solid depends on the *hyperelastic potential* $\mathscr{W}^e = \mathscr{W}^e(\underline{\underline{C}})$ and, in the case of *isotropic* material, we have

$$\mathscr{W}^e = \mathscr{W}^e(I_1, I_2, I_3) \quad s.t. \quad \underline{\underline{\Sigma}} = \frac{\partial \mathscr{W}^e}{\partial \underline{\underline{e}}}(I_1, I_2, I_3) = 2\sum_{i=1}^{3} \frac{\partial \mathscr{W}^e}{\partial I_i} \frac{\partial I_i}{\partial \underline{\underline{C}}}$$

where I_1, I_2, I_3 are the eigenvalues of $\underline{\underline{C}}(\underline{u})$ known as *invariants*

$$I_1 = \operatorname{tr} \underline{\underline{C}} \,, \qquad I_2 = \operatorname{tr}(\operatorname{cof} \underline{\underline{C}}) = \frac{1}{2}((\operatorname{tr} \underline{\underline{C}})^2 - \operatorname{tr}(\underline{\underline{C}}^2)) \,, \qquad I_3 = \det \underline{\underline{C}} = J^2 \,.$$

The application of this work concerns hyperelastic nearly-incompressible materials, like soft tissues characterized by high water content. A classical decomposition of the Second Piola Kirchhoff tensor $\underline{\underline{\Sigma}}$ is given by the definition of the hydrostatic pressure p and the deviatoric component $\underline{\underline{\Sigma}}^d$

$$p = -\frac{1}{3J}\underline{\underline{\Sigma}} : \underline{\underline{C}} \quad \text{and} \quad \underline{\underline{\Sigma}}^d = \underline{\underline{\Sigma}} + pJ\underline{\underline{C}}^{-1} \qquad s.t. \quad \underline{\underline{\Sigma}} = \underline{\underline{\Sigma}}^d - pJ\underline{\underline{C}}^{-1} \,. \tag{9}$$

The stress tensor is thereby decomposed in its deviatoric and volumetric term, and in particular we have $\underline{\underline{\Sigma}}^d : \underline{\underline{C}} = 0$ (volumetric deformation do not generate any work from the deviatoric component).

The nearly-incompressibility is taken into account with an additional strain energy density that constraints volume changes. This term can be interpreted as a dilatation strain energy function that depends only on I_3, for which a small variation in volume is penalized by a large bulk modulus. However, to achieve a separation in the energy density function between the component related to distortion and dilatation deformation [**Penn1970**, **Chen1996**], we cannot use I_1 and I_2 as they are not fully isochoric. We introduce the *reduced invariants*

$$J_1 = I_1 I_3^{-1/3}, \quad J_2 = I_2 I_3^{-2/3}, \quad J_3 = I_3^{1/2} = J \tag{10}$$

and we do the classical splitting

$$\mathscr{W}^e(I_1, I_2, I_3) = \mathscr{W}^d(J_1, J_2) + \mathscr{W}^v(J) \,,$$

where $\mathscr{W}^d(J_1, J_2)$ and $\mathscr{W}^v(J_3)$ correspond respectively to the elastic potential referred to deviatoric and volumetric deformations. We suggest the reader to look in [**Chang1991**] for further details. From definitions (9), we derive that

$$p(J) = -\frac{\mathrm{d}\mathscr{W}^v(J)}{\mathrm{d}J} \qquad \text{and} \qquad \underline{\underline{\Sigma}}^d = 2\sum_{i=1}^{2} \frac{\partial \mathscr{W}^d}{\partial J_i} \frac{\partial J_i}{\partial \underline{\underline{C}}} \,.$$

Consequently, we can specify an equivalent formulation of (8), with the additional term related to volumetric deformation. It reads:

For any $t \in [0; T]$ find $\underline{u}(t) \in \mathcal{W}$ such that

$$\begin{aligned} \int_{\widehat{\Omega}} \widehat{\varrho}\, \partial_{tt}\underline{u} \cdot \underline{\widehat{v}} \,\mathrm{d}\widehat{\Omega} + \int_{\widehat{\Omega}} \left(\underline{\underline{\Sigma}}^d(\underline{\underline{e}}(\underline{u})) - pJ\underline{\underline{C}}^{-1} \right) : \mathrm{D}\underline{\underline{e}}(\underline{u}) \cdot \underline{\widehat{v}} \,\mathrm{d}\widehat{\Omega} \\ = \int_{\widehat{\Omega}} \widehat{\varrho}\underline{\widehat{f}} \cdot \underline{\widehat{v}} \,\mathrm{d}\widehat{\Omega} + \int_{\widehat{\Gamma}_N} \underline{\widehat{t}} \cdot \underline{\widehat{v}} \,\mathrm{d}\hat{s} \end{aligned} \qquad \forall\, \underline{\widehat{v}} \in \mathcal{V}(\widehat{\Omega}) \,. \tag{11}$$

We recall that in (11) the terms p, J and $\underline{\underline{C}}$ are function of the unknown solution $\underline{u}$, while $\widehat{\varrho}, \underline{\widehat{f}}$ and $\underline{\widehat{t}}$ are given parameters.

2.2 Elastic wave propagation in quasi-static loaded solid

Let us now consider that the load applied to the solid is defined as follows

$$\widehat{\underline{f}}(\underline{\xi},t) = \widehat{\underline{f}}_0(\underline{\xi}) + \delta\widetilde{\underline{f}}(\underline{\xi},t) \tag{12}$$

The solid undergoes large deformation due to the application of the quasi-static load $\widehat{\underline{f}}_0(\underline{\xi})$, and it is subjected to a transient small-amplitude perturbation $\delta\widetilde{\underline{f}}(\underline{\xi},t)$ with δ as a small parameter, that generates the wave propagation. Solutions can be written as

$$\underline{u}(\underline{\xi},t) = \underline{u}_0(\underline{\xi}) + \delta\widetilde{\underline{u}}(\underline{\xi},t) + \mathcal{O}(\delta^2)\ , \tag{13}$$

where $\underline{u}_0$ is the governing solution of the quasi-static non-linear mechanics and $\delta\widetilde{\underline{u}}$ is the small-amplitude wave propagating in the loaded configuration.

2.2.1 Wave propagation problem in the reference configuration

With the external load defined as in (12) we derive the governing equation for the small perturbation $\widetilde{\underline{u}}$, i.e. the wave propagation, by linearizing (8) around the static loaded configuration given by the displacement $\underline{u}_0$.

We start the process of linearization with the component related to the deviatoric component of the internal work

$$\int_{\widehat{\Omega}} \underline{\underline{\Sigma}}^d(\underline{\underline{e}}(\underline{u})) : \mathrm{D}\underline{\underline{e}}(\underline{u}) \cdot \widehat{\underline{v}}\ \mathrm{d}\widehat{\Omega} \tag{14}$$

First, we linearize the derivative of the Green-Lagrange strain tensor

$$\mathrm{D}\underline{\underline{e}}(\underline{u}) \cdot \widehat{\underline{v}} = \mathrm{D}\underline{\underline{e}}(\underline{u}_0) \cdot \widehat{\underline{v}} \ + \ \delta\mathrm{D}^2\,\underline{\underline{e}}(\widetilde{\underline{u}},\widehat{\underline{v}}) \ + \ \mathcal{O}(\delta^2) \tag{15}$$

with

$$\mathrm{D}^2\,\underline{\underline{e}}(\widetilde{\underline{u}},\widehat{\underline{v}}) := \frac{1}{2}\left(\underline{\underline{\nabla}}_\xi\widetilde{\underline{u}}^T\underline{\underline{\nabla}}_\xi\widehat{\underline{v}} + \underline{\underline{\nabla}}_\xi\widehat{\underline{v}}^T\underline{\underline{\nabla}}_\xi\widetilde{\underline{u}}\right)$$

For the linearization of the deviatoric component of the stress tensor $\underline{\underline{\Sigma}}^d$, let us first introduce some useful notation that we will use for the rest of the paper

$$\mathrm{D}\underline{\underline{e}}_0(\underline{w}) := \mathrm{D}\underline{\underline{e}}_0(\underline{w}) \circ \underline{\phi}(\underline{\xi}) := \mathrm{D}\underline{\underline{e}}(\underline{u}_0) \cdot \underline{w} = \frac{1}{2}\left(\underline{\underline{\nabla}}_\xi\underline{w}^T \cdot \underline{\underline{F}}_0 + \underline{\underline{F}}_0^T \cdot \underline{\underline{\nabla}}_\xi\underline{w}\right) \tag{16}$$

$$\mathbf{C}_0^d : \underline{\underline{s}} \ := \mathrm{D}\underline{\underline{\Sigma}}^d(\underline{\underline{e}}(\underline{u}_0)) : \underline{\underline{s}} \qquad \text{(Gateaux derivative)} \tag{17}$$

where $\underline{\underline{F}}_0 = \underline{\underline{F}}(\underline{u}_0)$ and the first order derivative of $\underline{\underline{e}}$ evaluated in $\underline{u}_0$ in the direction $\underline{w}$ is now denoted with $\mathrm{D}\underline{\underline{e}}_0(\underline{w})$. The 4th-order tensor $\mathbf{C}_0^d$ is characterized by minor and major symmetries, and it accounts for the deviatoric behavior of the solid at the quasi-static configuration defined by $\underline{u}_0$. The linearization of the deviatoric stress reads

$$\underline{\underline{\Sigma}}^d(\underline{\underline{e}}(\underline{u})) = \underline{\underline{\Sigma}}_0^d + \delta\widetilde{\underline{\underline{\Sigma}}}^d + \mathcal{O}(\delta^2) \qquad \text{with} \qquad \begin{cases} \underline{\underline{\Sigma}}_0^d := \underline{\underline{\Sigma}}^d(\underline{\underline{e}}(\underline{u}_0)) \\ \widetilde{\underline{\underline{\Sigma}}}^d := \mathbf{C}_0^d : \mathrm{D}\underline{\underline{e}}_0(\widetilde{\underline{u}}) \end{cases} \tag{18}$$

Finally, due to the symmetry of $\underline{\underline{\Sigma}}^d$ and $\mathbf{C}_0^d$, we write

$$\begin{aligned} &\int_{\widehat{\Omega}} \underline{\underline{\Sigma}}^d(\underline{\underline{e}}(\underline{u})) : \mathrm{D}\underline{\underline{e}}(\underline{u}) \cdot \widehat{\underline{v}}\, d\widehat{\Omega} = \\ &= \int_{\widehat{\Omega}} \underline{\underline{\Sigma}}_0^d : \mathrm{D}\underline{\underline{e}}_0(\widehat{\underline{v}})\, \mathrm{d}\widehat{\Omega} \ + \delta\left[\int_{\widehat{\Omega}} \mathrm{D}\underline{\underline{e}}_0(\widetilde{\underline{u}}) : \mathbf{C}_0^d : \mathrm{D}\underline{\underline{e}}_0(\widehat{\underline{v}})\ \mathrm{d}\widehat{\Omega} \ + \int_{\widehat{\Omega}} \underline{\underline{\Sigma}}_0^d : \underline{\underline{\nabla}}_\xi\widetilde{\underline{u}}^T\underline{\underline{\nabla}}_\xi\widehat{\underline{v}}\, \mathrm{d}\widehat{\Omega}\right] + \mathcal{O}(\delta^2). \end{aligned} \tag{19}$$

Let us now present the linearization of the volumetric stress term

$$\int_{\widehat{\Omega}} pJ\underline{\underline{C}}^{-1} : \mathrm{D}\underline{\underline{e}}(\underline{u}) \cdot \underline{\widehat{v}} \, \mathrm{d}\widehat{\Omega}.$$

We linearize all terms dependent on $\underline{u}$ as follows

$$\underline{\underline{C}}^{-1} = \underline{\underline{C}}_0^{-1} + \delta\underline{\underline{\widetilde{G}}} \qquad \text{with} \qquad \begin{cases} \underline{\underline{C}}_0^{-1} = \underline{\underline{C}}(\underline{u}_0)^{-1} \\ \underline{\underline{\widetilde{G}}} = -2\, \underline{\underline{C}}_0^{-1} \cdot \mathrm{D}\underline{\underline{e}}_0(\underline{\widetilde{u}}) \cdot \underline{\underline{C}}_0^{-1} \end{cases}$$

$$J = J_0 + \delta\tilde{J} \qquad \text{with} \qquad \begin{cases} J_0 = [\det(\underline{\underline{C}}_0)]^{1/2} \\ \tilde{J} = J_0\, \underline{\underline{C}}_0^{-1} : \mathrm{D}\underline{\underline{e}}_0(\underline{\widetilde{u}}) \end{cases}$$

$$p = p_0 + \delta\tilde{p} \qquad \text{with} \qquad \begin{cases} p_0 = p(J_0) = -\dfrac{\mathrm{d}\mathscr{W}^v}{\mathrm{d}J}(J_0) \\ \tilde{p} = \dfrac{\mathrm{d}p}{\mathrm{d}J}(J_0)\tilde{J} = -\dfrac{\mathrm{d}^2\mathscr{W}^v}{\mathrm{d}J^2}(J_0)\; J_0\underline{\underline{C}}_0^{-1} : \mathrm{D}\underline{\underline{e}}_0(\underline{\widetilde{u}}). \end{cases}$$

From these results and the previous linearization of the deformation tensor, the volumetric term reads

$$\begin{aligned} \int_{\widehat{\Omega}} pJ\underline{\underline{C}}^{-1} :\, \mathrm{D}\underline{\underline{e}}(\underline{u}) \cdot \underline{\widehat{v}}\, d\widehat{\Omega} = \int_{\widehat{\Omega}} p_0 J_0 \underline{\underline{C}}_0^{-1} : \mathrm{D}\underline{\underline{e}}_0(\underline{\widehat{v}})\, \mathrm{d}\widehat{\Omega} + \\ + \;\delta\Big[\int_{\widehat{\Omega}} (\tilde{p}J_0 + p_0\tilde{J})\underline{\underline{C}}_0^{-1} : \mathrm{D}\underline{\underline{e}}_0(\underline{\widehat{v}})\; \mathrm{d}\widehat{\Omega} + \int_{\widehat{\Omega}} p_0 J_0 \underline{\underline{\widetilde{G}}} : \mathrm{D}\underline{\underline{e}}_0(\underline{\widehat{v}})\; \mathrm{d}\widehat{\Omega} \\ + \int_{\widehat{\Omega}} p_0 J_0 \underline{\underline{C}}_0^{-1} : \underline{\underline{\nabla}}_\xi \underline{\widetilde{u}}^T \underline{\underline{\nabla}}_\xi \underline{\widehat{v}}\, \mathrm{d}\widehat{\Omega}\Big] + \mathcal{O}(\delta^2)\,. \end{aligned} \tag{20}$$

The linearization of the inertial term takes into account the static condition of the non-linear solution, hence we have:

$$\int_{\widehat{\Omega}} \widehat{\varrho}\; \partial_{tt}\underline{u} \cdot \underline{\widehat{v}}\, \mathrm{d}\widehat{\Omega} = \delta \int_{\widehat{\Omega}} \widehat{\varrho}\; \partial_{tt}\underline{\widetilde{u}} \cdot \underline{\widehat{v}}\, \mathrm{d}\widehat{\Omega}\,.$$

Let us now separate the non-linear static part from the linear part of the problem, in order to distinguish the different physics of the problem for which we will need different methods of approximation. We also assume no surface traction for the sake of simplicity ($\underline{t} = 0$).

Quasi-static problem *The non-linear problem in the reference configuration reads:*
Find $\underline{u}_0 \in \mathcal{W}(\widehat{\Omega})$ *such that*

$$\begin{cases} \displaystyle\int_{\widehat{\Omega}} \left(\underline{\underline{\Sigma}}_0^d - p_0 J_0 \underline{\underline{C}}_0^{-1}\right) : \mathrm{D}\underline{\underline{e}}_0(\underline{\widehat{v}})\, \mathrm{d}\widehat{\Omega} = \int_{\widehat{\Omega}} \widehat{\varrho}\underline{\widehat{f}}_0 \cdot \underline{\widehat{v}}\, \mathrm{d}\widehat{\Omega} \quad \forall\, \underline{\widehat{v}} \in \mathcal{V}(\widehat{\Omega}) \\ \displaystyle p_0 = -\frac{\mathrm{d}\mathscr{W}^v}{\mathrm{d}J}(J_0) \end{cases} \tag{21}$$

We recall that the Second Piola Kirchhoff evaluated at $\underline{u}_0$, that will be referred to as the prestress is

$$\underline{\underline{\Sigma}}_0 := \underline{\underline{\Sigma}}(\underline{u}_0) = \underline{\underline{\Sigma}}_0^d - p_0 J_0 \underline{\underline{C}}_0^{-1}\,. \tag{22}$$

Once the non-linear solution is given, we obtain the wave propagation in the quasi-static loaded solid by solving the linearized problem, following

Wave equation in reference configuration *For any* $t \in [0,T]$, *find* $\widetilde{\underline{u}}(t) \in \mathcal{V}(\widehat{\Omega})$ *such that*

$$\begin{cases} \displaystyle\int_{\widehat{\Omega}} \widehat{\varrho}\, \partial_{tt}\widetilde{\underline{u}} \cdot \widehat{\underline{v}}\, \mathrm{d}\widehat{\Omega} + \int_{\widehat{\Omega}} \mathrm{D}\underline{\underline{e}}_0(\widetilde{\underline{u}}) : \mathbf{C}_0^d : \mathrm{D}\underline{\underline{e}}_0(\widehat{\underline{v}})\ \mathrm{d}\widehat{\Omega} \\ \qquad + 2\displaystyle\int_{\widehat{\Omega}} p_0\, J_0\, \underline{\underline{C}}_0^{-1} \cdot \mathrm{D}\underline{\underline{e}}_0(\widetilde{\underline{u}}) : \underline{\underline{C}}_0^{-1} \cdot \mathrm{D}\underline{\underline{e}}_0(\widehat{\underline{v}})\ \mathrm{d}\widehat{\Omega} \qquad \forall \widehat{\underline{v}} \in \mathcal{V}(\widehat{\Omega}) \\ \qquad + \displaystyle\int_{\widehat{\Omega}} \lambda^* \underline{\underline{C}}_0^{-1} : \mathrm{D}\underline{\underline{e}}_0(\widetilde{\underline{u}})\ \underline{\underline{C}}_0^{-1} : \mathrm{D}\underline{\underline{e}}_0(\widehat{\underline{v}})\ \mathrm{d}\widehat{\Omega} \\ \qquad + \displaystyle\int_{\widehat{\Omega}} \underline{\underline{\Sigma}}_0 : \underline{\underline{\nabla}}_\xi \widetilde{\underline{u}}^T \underline{\underline{\nabla}}_\xi \widehat{\underline{v}}\, \mathrm{d}\widehat{\Omega} = \displaystyle\int_{\widehat{\Omega}} \widehat{\widetilde{\varrho}}\, \widehat{\underline{f}} \cdot \widehat{\underline{v}}\, \mathrm{d}\widehat{\Omega} \end{cases} \tag{23}$$

where

$$\lambda^* := -J_0^2 \frac{\mathrm{d}p}{\mathrm{d}J}(J_0) - J_0 p_0 = J_0 \left(J_0 \frac{\mathrm{d}^2 \mathscr{W}^v}{\mathrm{d}J^2}(J_0) + \frac{\mathrm{d}\mathscr{W}^v}{\mathrm{d}J}(J_0) \right)$$

with initial condition

$$\widetilde{\underline{u}}(0) = 0, \qquad \partial_t \widetilde{\underline{u}}(0) = 0$$

We remark that the parameter λ^* will have a high value as the bulk modulus of the potential $\mathscr{W}^v$ is taken very large to enforce the incompressibility.

2.2.2 Wave propagation problem in the apparent configuration

In an application framework, the wave propagation is measured in the loaded configuration described by $\underline{u}_0$. It is useful, indeed, to reformulate the linearized problem in the quasi-static loaded configuration denoted with Ω_0, whose set of points $\underline{x}_0$ can be retrieved with the bijective deformation map $\underline{\phi}_0(\underline{\xi})$:

$$\underline{\phi}_0 : \underline{\xi} \to \underline{x}_0(\underline{\xi}) = \underline{\phi}_0(\underline{\xi})$$

$$\underline{\phi}_0(\underline{\xi}) = \underline{u}_0(\underline{\xi}) + \underline{\xi}$$

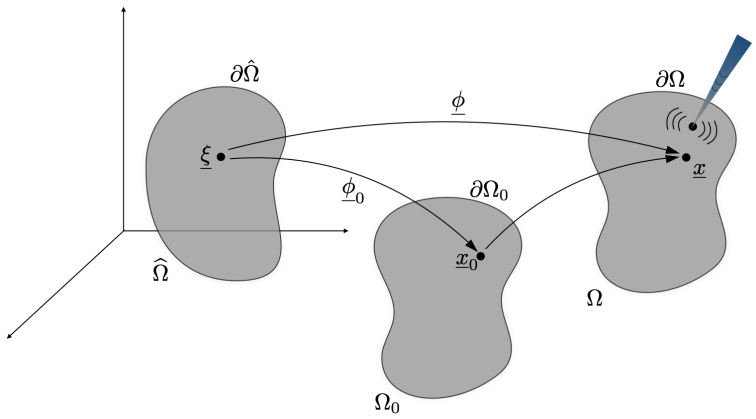

Figure 1. Reference $\widehat{\Omega}$, apparentΩ_0 and deformed Ω configurations related by the respective deformation maps

We also introduce the functional space $\mathcal{V}(\Omega_0) := \{\underline{v} \in \mathrm{H}^1(\Omega_0)^d\}$ where we seek the solution of the linear solution. Given a function $\underline{w}$ defined in Ω_0, we can define the linear strain tensor in the apparent configuration as

$$\underline{\underline{\varepsilon}}_{\underline{x}_0}(\underline{w}) = \frac{1}{2}(\underline{\underline{\nabla}}_{\underline{x}_0}\underline{w} + \underline{\underline{\nabla}}_{\underline{x}_0}\underline{w}^T). \tag{24}$$

We now want to refer the mechanical quantities of the wave equation (23) with respect to Ω_0. We combine (3) and (16) to write the first order derivative of Green-Lagrange strain tensor evaluated in $\underline{u}_0$ w.r.t. the apparent configuration Ω_0

$$(\mathrm{D}\underline{\underline{e}}_0(\underline{w}\circ\underline{\phi}_0)\circ\underline{\phi}_0^{-1})(\underline{x}_0) = \frac{1}{2}\left(\underline{\underline{F}}_0^T\cdot\underline{\underline{\nabla}}_{\underline{x}_0}\underline{w}^T\cdot\underline{\underline{F}}_0 + \underline{\underline{F}}_0^T\cdot\underline{\underline{\nabla}}_{\underline{x}_0}\underline{w}\cdot\underline{\underline{F}}_0\right) = \underline{\underline{F}}_0^T\cdot\underline{\underline{\varepsilon}}_{\underline{x}_0}(\underline{w})\cdot\underline{\underline{F}}_0$$

From this relation one can derive thw two equation below that are used to treat the terms related to the linearization of the volumetric work, in the apparent configuration we have

$$(\underline{\underline{C}}_0^{-1} : \mathrm{D}\underline{\underline{e}}_0(\underline{w}\circ\underline{\phi}_0))\circ\underline{\phi}_0^{-1} = \underline{\underline{\mathbb{1}}} : \underline{\underline{\varepsilon}}_{\underline{x}_0}(\underline{w}) = \mathrm{div}_{\underline{x}_0}\underline{w},$$

$$(\underline{\underline{C}}_0^{-1}\cdot\mathrm{D}\underline{\underline{e}}_0(\widetilde{\underline{u}}) : \underline{\underline{C}}_0^{-1}\cdot\mathrm{D}\underline{\underline{e}}_0(\underline{w}\circ\underline{\phi}_0))\circ\underline{\phi}_0^{-1} = \underline{\underline{\varepsilon}}_{\underline{x}_0}(\widetilde{\underline{u}}\circ\underline{\phi}_0^{-1}) : \underline{\underline{\varepsilon}}_{\underline{x}_0}(\underline{w}).$$

With the relation between the Cauchy tensor and the second Piola Kircchoff (5), we bring in the apparent configuration the term depending on the pre-stress $\underline{\underline{\Sigma}}_0$

$$(\underline{\underline{\Sigma}}_0 : \underline{\underline{\nabla}}_{\underline{\xi}}\widetilde{\underline{u}}^T\underline{\underline{\nabla}}_{\underline{\xi}}(\underline{w}\circ\underline{\phi}_0))\circ\underline{\phi}_0^{-1} = J_0\,\underline{\underline{\nabla}}_{\underline{x}_0}(\widetilde{\underline{u}}\circ\underline{\phi}_0^{-1})\cdot\underline{\underline{\sigma}}_0 : \underline{\underline{\nabla}}_{\underline{x}_0}\underline{w}$$

$$\text{with}\quad \underline{\underline{\sigma}}_0 := \underline{\underline{\sigma}}(\underline{u}_0)\circ\underline{\phi}_0^{-1} = (J_0^{-1}\underline{\underline{F}}_0\cdot\underline{\underline{\Sigma}}_0\cdot\underline{\underline{F}}_0^T)\circ\underline{\phi}_0^{-1}$$

For the sake of lightening the reading, we will now drop the notation "$\cdot\circ\underline{\phi}_0^{-1}$".

We now use (2) considering the deformation map $\underline{\phi}_0$ between $\widehat{\Omega}$ and Ω_0, in order to obtain the formulation of the elastic wave propagation problem in the apparent configuration, which reads:

Wave equation in apparent configuration Ω_0: *For any $t \in [0,T]$, find $\widetilde{\underline{u}}(t) \in \mathcal{V}(\Omega_0)$ such that*

$$\begin{cases} \displaystyle\int_{\Omega_0} \varrho_0 \partial_{tt}\widetilde{\underline{u}} \cdot \underline{v}\ \mathrm{d}\Omega_0 \ + \int_{\Omega_0} \underline{\underline{\varepsilon}}_{\underline{x}_0}(\widetilde{\underline{u}}) : \widetilde{\mathbf{C}}_0 : \underline{\underline{\varepsilon}}_{\underline{x}_0}(\underline{v})\ \mathrm{d}\Omega_0 \\ + \displaystyle\int_{\Omega_0} \underline{\underline{\nabla}}_{\underline{x}_0}\widetilde{\underline{u}}\ \underline{\underline{\sigma}}_0 : \underline{\underline{\nabla}}_{\underline{x}_0}\underline{v}\ \mathrm{d}\Omega_0 \qquad\qquad \forall \underline{v} \in \mathcal{V}(\Omega_0) \\ + \displaystyle\int_{\Omega_0} \lambda_0^* \mathrm{div}_{\underline{x}_0}(\widetilde{\underline{u}})\mathrm{div}_{\underline{x}_0}(\underline{v})\mathrm{d}\Omega_0 = \int_{\Omega_0} \varrho_0 \underline{\tilde{f}} \cdot \underline{v}\ \mathrm{d}\Omega_0 \end{cases} \tag{25}$$

where

$$\begin{aligned} &\widetilde{\mathbf{C}}_0 : \underline{\underline{s}} := J_0^{-1}\underline{\underline{F}}_0\Big(\mathbf{C}_0^d : \underline{\underline{F}}_0^T\,\underline{\underline{s}}\,\underline{\underline{F}}_0\Big)\underline{\underline{F}}_0^T + 2\,p_0\,\underline{\underline{s}} \\ &\lambda_0^* := J_0^{-1}\lambda^* = J_0\frac{\mathrm{d}^2\mathscr{W}^v}{\mathrm{d}J^2}(J_0) + \frac{\mathrm{d}\mathscr{W}^v}{\mathrm{d}J}(J_0) \\ &\varrho_0 := J_0^{-1}\widehat{\varrho} \end{aligned} \tag{26}$$

with initial condition

$$\widetilde{\underline{u}}(0) = 0 \qquad \partial_t\widetilde{\underline{u}}(0) = 0$$

We can then distinguish three stiffness terms that affect the propagation of the wave:

- the material stiffness given by the linearized material behavior around a loaded configuration
$$\int_{\Omega_0} \underline{\underline{\varepsilon}}_{\underline{x}_0}(\widetilde{\underline{u}}) : \widetilde{\mathbf{C}}_0 : \underline{\underline{\varepsilon}}_{\underline{x}_0}(\underline{v})\ \mathrm{d}\Omega_0$$
- the geometric stiffness depending on the prestress resulting from the non-linear static problem
$$\int_{\Omega_0} \underline{\underline{\nabla}}_{x_0}\widetilde{\underline{u}}\ \underline{\underline{\sigma}}(\underline{u}_0) : \underline{\underline{\nabla}}_{x_0}\underline{v}\ \mathrm{d}\Omega_0$$
- the volumetric stiffness that corresponds to the Grad-div operator
$$\int_{\Omega_0} \lambda^* \mathrm{div}_{\underline{x}_0}(\widetilde{\underline{u}})\mathrm{div}_{\underline{x}_0}(\underline{v})\mathrm{d}\Omega_0$$
where λ^* only depends on the chosen energy density function to penalize volumetric deformations.

As we mentioned at the beginning, the formulation of the problem in the apparent configuration Ω_0 is useful to isolate the term related to the nearly-incompressibility and develop a numerical strategy capable of overcoming the limitations related to this constraint.

2.2.3 An example of strain energy function for nearly incompressible material

Let us now consider an example of penalization term for nearly-incompressible solids, as the one proposed in [**Ciarlet1982lois**]

$$\mathscr{W}^v = k(J-1) - k\log(J)$$

where $k \in \mathbb{R}^+$ is the bulk modulus taken very large with respect to other material parameters. The stress related to the volumetric deformation will be defined

$$\underline{\underline{\Sigma}}^v = -pJ\underline{\underline{C}}^{-1} \qquad \text{with} \quad p = k\frac{1-J}{J}$$

and its linearization results in

$$\underline{\underline{\Sigma}}^v = -pJ\underline{\underline{C}}^{-1} = k[(J_0\underline{\underline{C}}_0^{-1} - \underline{\underline{C}}_0^{-1}) + \delta((J_0-1)\widetilde{\underline{\underline{G}}} + \tilde{J}\underline{\underline{C}}_0^{-1})]$$

We derive from (21) and (23) that

$$p_0 = k\frac{1-J_0}{J_0} \qquad \text{and} \qquad \lambda^* = k\ ,$$

such that the shear term will be characterized by the following material stiffness

$$\widetilde{\mathbf{C}}_0 : \underline{\underline{\varepsilon}}_{\underline{x}_0}(\widetilde{\underline{u}}) := J_0^{-1}\underline{\underline{F}}_0\Big(\mathbf{C}_0^d : \underline{\underline{F}}_0^T\underline{\underline{\varepsilon}}_{\underline{x}_0}(\widetilde{\underline{u}})\ \underline{\underline{F}}_0\Big)\underline{\underline{F}}_0^T + 2\,k\frac{1-J_0}{J_0}\,\underline{\underline{\varepsilon}}_{\underline{x}_0}(\widetilde{\underline{u}})$$

and the term related to the pressure propagation corresponds to

$$\int_{\Omega_0} k\ \mathrm{div}_{\underline{x}_0}(\widetilde{\underline{u}})\mathrm{div}_{\underline{x}_0}(\underline{v})\mathrm{d}\Omega_0\ .$$

We remark that the internal pressure p_0 could be a source of instability, since it is negative for non-linear problems characterized by volumetric increase. Furthermore, it has been seen that wave propagation problems obtained by linearization may suffer from loss of coercivity, depending on the chosen elastic potential and the static solution $\underline{u}_0$. To avoid a possible buckling issue, a check of the smallest eigenvalues of the stiffness operator should be performed. Further discussions concerning these aspects can be found in [**Dalmora2023**].

For the purpose of our problem, we will strongly penalize any volumetric deformation due to nearly-incompressibility, hence we can assume the total tangent stiffness term to be coercive.

3 A fully explicit numerical scheme

The scope of this section is to propose a numerical scheme for the computation of the elastic wave propagation problem in a nearly-incompressible linearized solid. We will present the scheme considering the solid at, rest in order to simplify the presentation and highlight the main aspects of the scheme. We remark that this assumption doesn't affect the applicability of the scheme, since the operator related to the enforcement of incompressibility (the grad-div operator) is not affected by the preload, beside the parameter λ^* which – although it may vary in space in general – is homogeneous for the specific case presented Section 2.2.3. In more complicated situations, since in practice the parameter λ^* is large it acts as a penalization parameter and can be approximated by a constant value. Therefore, in what follows we assume that

$$\lambda^* = \lambda \quad \text{with} \quad \nabla\lambda = 0.$$

Given the linearity of the problem it is equivalent to write equation with lagrangian or eulerian formalism, such that we will write the wave propagation problem in the configuration Ω. Once we have introduced the linear continuous operators associated to our problem, we will introduce a strategy for space discretization focused on the accuracy and the efficiency of the numerical approximation. Finally, a fully explicit method for the time-discretization is given. The method is based on a classical LF scheme together with the use of Chebyshev polynomials (as proposed in [**Carle2020**]), for the relaxation of the CFL condition in the novel application of nearly-incompressible solids.

3.1 Linearization at rest condition

For the presentation of the numerical scheme, we consider the case of a hyperelastic solid, linearized around at rest condition, such that the displacement field (13) reduces to $\underline{u}(\underline{x},t) = \widetilde{\underline{u}}(\underline{x},t)$.

We rewrite the formulation (25) as a set of equations in $\mathcal{V}'$, the dual space of the Hilbert space

$$\mathcal{V} = \mathcal{V}(\Omega) = \{\underline{v} \in \mathrm{H}^1(\Omega)^d \mid \underline{v} = 0 \text{ on } \Gamma_D\}.$$

Note that the scalar product on $\mathcal{V}$ is the standard $H^1(\Omega)$ scalar product. Let us define the bilinear form $m : \mathcal{V} \times \mathcal{V} \to \mathbb{R}$ and related linear continuous operator $M : \mathcal{V} \to \mathcal{V}'$ as

$$m(\underline{u},\underline{v}) := \langle M\underline{u},\underline{v}\rangle_{\mathcal{V}',\mathcal{V}} := \int_\Omega \varrho\underline{u}\cdot\underline{v}\ \mathrm{d}\Omega.$$

defined in $\mathrm{L}^2(\Omega)$ space. Notice that this bilinear form is symmetric and coercive in $L^2(\Omega)^3$.

The bilinear form $a : \mathcal{V} \times \mathcal{V} \to \mathbb{R}$ is rewritten as the sum of two bilinear forms, one contributing to the shear-waves propagation $a_s : \mathcal{V} \times \mathcal{V} \to \mathbb{R}$ and another one contributing to pressure wave propagation $a_p : \mathcal{V} \times \mathcal{V} \to \mathbb{R}$. To these bilinear forms we associate linear continuous operators A^s and $A^p : \mathcal{V} \to \mathcal{V}'$ defined by

$$a_s(\underline{u},\underline{v}) := \langle A^s\underline{u},\underline{v}\rangle_{\mathcal{V}',\mathcal{V}} := \int_\Omega \underline{\underline{\varepsilon}}(\underline{u}) : \mathbf{C}^d : \underline{\underline{\varepsilon}}(\underline{v})\ \mathrm{d}\Omega,$$
$$a_p(\underline{u},\underline{v}) := \langle A^p\underline{u},\underline{v}\rangle_{\mathcal{V}',\mathcal{V}} := \int_\Omega \mathrm{div}(\underline{u})\,\mathrm{div}(\underline{v})\ \mathrm{d}\Omega.$$

The bilinear form $a(\cdot,\cdot) = a_s(\cdot,\cdot) + a_p(\cdot,\cdot)$ is continuous and weakly coercive i.e. $\exists\, c, C \in \mathbb{R}^+$ such that

$$c||v||_{\mathcal{V}}^2 \leq \|v\|_{L^2(\Omega)}^2 + |a(v,v)| \quad \text{and} \quad |a(u,v)| \leq C||u||_{\mathcal{V}}||v||_{\mathcal{V}}$$

while the symmetry is easily verified by looking at definition of $a_s(\cdot,\cdot)$ and $a_p(\cdot,\cdot)$. Under these assumptions, the wave propagation problem of (25) linearized around at rest condition reads:

For any $t \in [0,T]$, find $\underline{u}(t) \in \mathcal{V}$ such that

$$M\partial_{tt}\underline{u} + A^s\underline{u} + \lambda A^p\underline{u} = \underline{f} \quad \text{in } \mathcal{V}' \quad \text{and} \quad \underline{u}(0) = \partial_t\underline{u}(0) = 0 \quad \text{in } \Omega. \tag{NI}$$

Existence results of a unique solution for this problem are given for instance in [**joly2007numerical**].

Let us now present an equivalent formulation with the introduction of the pressure $p := \lambda\,\mathrm{div}\,\underline{u}$ as a second variable of the problem. We denote with $\mathcal{L}$ the function space of the scalar pressure field

$$\mathcal{L} := \{q \in \mathrm{L}^2(\Omega)\},$$

and we define the bilinear form $d : \mathcal{L} \times \mathcal{V} \to \mathbb{R}$, with the related divergence operator $D : \mathcal{V} \to \mathcal{L}$ and its adjoint gradient operator $D^* : \mathcal{L} \to \mathcal{V}'$, such that $\forall(\underline{u}, q) \in \mathcal{V} \times \mathcal{L}$

$$d(q, \underline{u}) := \langle D^* q, \underline{u} \rangle_{\mathcal{V}',\mathcal{V}} := (q, D\,\underline{u})_{\mathcal{L}} := \int_\Omega q \,\mathrm{div}(\underline{u}) \,\mathrm{d}\Omega.$$

Note that the scalar product on $\mathcal{L}$ is the standard $L^2(\Omega)$ scalar product. Then, the *mixed formulation* reads: For any $t \in [0, T]$, find $(\underline{u}(t), p(t)) \in \mathcal{V} \times \mathcal{L}$ such that

$$\begin{cases} M\partial_{tt}\underline{u} + A^s\underline{u} + D^* p = \underline{f} & \text{in } \mathcal{V}' \\ D\underline{u} = \lambda^{-1}\, M^p\, p & \text{in } \mathcal{L} \end{cases} \quad \text{and} \quad \underline{u}(0) = \partial_t \underline{u}(0) = 0 \quad \text{in } \Omega \qquad \text{(NIM)}$$

with M^p is actually the identity map from $\mathcal{L} \to \mathcal{L}$. As we are dealing with a nearly-incompressible solid, it is interesting to notice that this latter formulation corresponds to a sort of penalization method for the resolution of the pure incompressible problem, where the pressure p would be a Lagrange multiplier [**Caforio2018**].

Comparing (NI) and (NIM) one can observe that

$$A^p = D^*(M^p)^{-1} D. \tag{27}$$

This observation has a discrete counterpart as shown in the Section below.

3.2 Space discretization

3.2.1 Semi-discret formulation

The classical method to solve finite-element approximation problem is known as displacement-based, which relies on the assumption that nodal displacements completely define the displacement of the body and are indeed the unknowns of the problem [**Bathe2006**, **Sussman1987**]. This nodal displacements belongs to finite-dimensional space $\mathcal{V}_h \subset \mathcal{V}$ that is a space of piecwise smooth and globally continuous functions. The space $\mathcal{V}_h$ is equipped with the scalar product

$$(\underline{u}_h, \underline{v}_h)_{\mathcal{H}} := \int_\Omega \underline{u}_h \cdot \underline{v}_h \,\mathrm{d}\Omega.$$

In order to derive the semi-discretized problem, we define the linear operators $M_h : \mathcal{V}_h \to \mathcal{V}_h$, $A^s_h : \mathcal{V}_h \to \mathcal{V}_h$ and $A^p_h : \mathcal{V}_h \to \mathcal{V}_h$ such that $\forall(\underline{u}_h, \underline{v}_h) \in \mathcal{V}_h \times \mathcal{V}_h$

$$(M_h\underline{u}_h, \underline{v}_h)_{\mathcal{H}} = \oint_\Omega \varrho\, \underline{u}_h \cdot \underline{v}_h \,\mathrm{d}\Omega \qquad (A^s_h\underline{u}_h, \underline{v}_h)_{\mathcal{H}} = \int_\Omega \mathbf{C}^d \underline{\underline{\varepsilon}}(\underline{u}_h) : \underline{\underline{\varepsilon}}(\underline{v}_h) \,\mathrm{d}\Omega$$

$$(A^p_h\underline{u}_h, \underline{v}_h)_{\mathcal{H}} = \int_\Omega \mathrm{div}\,\underline{u}_h \;\mathrm{div}\,\underline{v}_h \,\mathrm{d}\Omega$$

where the notation $\oint$ stands for the use of a quadrature formula for the computation of the integrals. The adequate quadrature formula to use depends on the choice of the finite element space $\mathcal{V}_h$ and is discussed later. The semi-discretized problem of (NI) reads: For any $t \in [0, T]$, find $\underline{u}_h(t) \in \mathcal{V}_h$ such that

$$M_h\partial_{tt}\underline{u}_h + A^s_h\underline{u}_h + \lambda A^p_h\underline{u}_h = \underline{f}_h \qquad \text{in } \mathcal{V}_h \tag{NId}$$

with null initial conditions and f_h an approximation of f in $\mathcal{V}_h$. However, it is well-known in finite element methods that the approximation of nearly-incompressible problems with a displacement based method suffers from several limitations, such as

need of highly-refined mesh, numerical locking (especially with low-order elements), ill-conditioning of the stiffness matrix and spurious pressure [**LeTallec1994**, **Bathe2006**, **Sussman1987**].

The classical technique to overcome these limitations is the *mixed method*, which relies on the interpolation of the pressure field in a separate finite element space, denoted here as $\mathcal{L}_h \subset \mathcal{L}$ equipped with the scalar product $(\cdot,\cdot)_{\mathcal{V}}$. Let us then consider the space discretization of the equivalent continuous problem defined with the mixed formulation (NIM). We introduce the discrete divergence operator $D_h : \mathcal{V}_h \to \mathcal{L}_h$ and its adjoint gradient operator $D_h^* : \mathcal{L}_h \to \mathcal{V}_h$ such that $\forall (\underline{u}_h, p_h) \in \mathcal{V}_h \times \mathcal{L}_h$

$$(D_h \underline{u}_h, p_h)_{\mathcal{L}} = (\underline{u}_h, D_h^* p_h)_{\mathcal{H}} \simeq \int_\Omega p_h \ \mathrm{div}\, \underline{u}_h \, \mathrm{d}\Omega. \tag{28}$$

Note that we are very vague at this point on the actual definition of the operator D_h. A precise description is given later in the manuscript. The spatial discretization of problem (NIM) reads:

For any time $t \in [0,T]$, find $(\underline{u}_h(t), p_h(t)) \in \mathcal{V}_h \times \mathcal{L}_h$ such that

$$\begin{cases} M_h \, \partial_{tt} \underline{u}_h + A_h^s \underline{u}_h + D_h^* p_h = \underline{f}_h & \text{in} \quad \mathcal{V}_h \\ D_h \underline{u}_h = \lambda^{-1} M_h^P p_h & \text{in} \quad \mathcal{L}_h \end{cases} \tag{29}$$

with null initial data and where M_h^P is the linear operator $\mathcal{L}_h \to \mathcal{L}_h$ given by

$$\forall\, (p_h, q_h) \in \mathcal{L}_h \times \mathcal{L}_h, \quad (M_h^P p_h, q_h)_{\mathcal{L}} = \oint_\Omega p_h q_h \mathrm{d}\Omega,$$

where – once again – a quadrature formula, adapted to the space $\mathcal{L}_h$ is used to compute the integral. By means of *Schur complement* method, we first compute the pressure field

$$p_h = \lambda (M_h^P)^{-1} D_h \underline{u}_h$$

and we obtain the *semi-discretized* scheme

$$M_h \partial_{tt} \underline{u}_h + A_h^s \underline{u}_h + \lambda \bar{A}_h^p \underline{u}_h = \underline{f}_h \qquad \text{with} \quad \bar{A}_h^p := D_h^* (M_h^P)^{-1} D_h. \tag{NIMd}$$

First observe that $\bar{A}_h^p$ is define using a discrete counterpart of the formula (27) for defining A^p. However – in general – the operator $\bar{A}_h^p$ differs from A_h^p unless some specific conditions are met. For instance, the two operators coincide when integral are computed exactly and $\mathrm{div}\, \mathcal{V}_h \subset \mathcal{L}_h$.

3.2.2 Spectral finite elements

Let us now assume our spatial domain Ω to be a geometry, such that we construct a quasi-uniform regular partition $\mathcal{T}_h$ of Ω, made of quadrangles ($d = 2$) or hexahedra ($d = 3$). Each deformed element $K \in \mathcal{T}_h$ is obtained with an invertible transformation $\underline{\phi}_K$ applied to the reference element $\hat{K} = [0,1]^d$.

This setting allows the use of high-order spectral finite element, for which we can apply the mass-lumping approach. The method [**Cohen2002**] consists in obtaining a diagonal mass matrix – which is trivial to invert – by choosing a quadrature rule which has quadrature points at the locations of the interpolation points of a Lagrangian basis of $\mathcal{V}_h$. The lagrangian basis is – as usual for finite elements – constructed locally on the reference element. On the reference element the basis is contructed using

Gauss-Lobatto points.

Furthermore, we recall that mixed variational problems are stable only for certain choices of finite element spaces that satisfy the *inf-sup* condition from the so-called Ladyzenskaya-Babuska-Brezzi theorem [**Babuvska1973**, **Brezzi1974**, **LeTallec1994**]. Unstable mixed methods are characterized by the appearance of nonphysical oscillations of the pressure field. The demonstration of the *inf-sup* condition is quite complex and out of the scope of this work. Hence, we rely on the analysis held in [**Pena2009**], in which a numerical analysis of convergences properties is presented for various choice of finite element spaces for $\mathcal{V}_h$ and $\mathcal{L}_h$.

We consider the $\mathcal{Q}_n - \mathcal{Q}_{n-2}^{disc}$ method, proposed by Maday et al. [**BernardiMaday1999**]. More precisely

$$\mathcal{V}_h = \{\varphi \in C^0(\Omega)^d \,|\quad \varphi|_K \circ \underline{\phi}_K \in \mathcal{Q}_n(\hat{K})^d\}, \tag{30}$$

$$\mathcal{L}_h = \{\psi \in L^2(\Omega) \,|\quad \psi|_K \circ \underline{\phi}_K \in \mathcal{Q}_{n-2}(\hat{K})\}. \tag{31}$$

This choice benefits of higher efficiency for the computation of the pressure field, given the lower order for the pressure field and the discontinuity of elements, for which the pressure contribution is computed locally. We remark that in 3D problems, the lower order of the shape functions for the pressure field results in the loss of one order of accuracy, that is comparable with the loss of one order already happenning on non-cartesian mesh due to mass-lumping [**Durufle2009**].

Note that, with the discussed choices, the operator M_h and M_h^P are computed using respectively a quadrature formula on the set of $(n+1)^d$ and $(n-1)^d$ Gauss-Lobatto points on the reference element.

Remark. *A first alternative would be the choice $\mathcal{Q}_n - \mathcal{Q}_{n-1}$ more precisely $\mathcal{L}_h$ is chosen as*

$$\mathcal{L}_h = \{\psi \in C^0(\Omega) \,|\quad \psi|_K \circ \underline{\phi}_K \in \mathcal{Q}_{n-1}(\hat{K})\}. \tag{32}$$

*This choice is analyzed in [***brezzi1991stability***], which are an extension of the widely used Taylor-Hood elements. They are characterized by optimal convergence properties but it more costly when computing local contributions. A second alternative is the choice $\mathcal{Q}_n - \mathcal{P}_{n-1}^{disc}$, for which*

$$\mathcal{L}_h = \{\psi \in C^0(\Omega) \,|\quad \psi|_K \circ \underline{\phi}_K \in \mathcal{P}_{n-1}(\hat{K})\}. \tag{33}$$

The choice has been discarded since it does not allow important optimization procedure related to the use of finite elements constructed on $\hat{K} = [0,1]^d$ by cartesian product (such as the spectral finite elements).

3.2.3 Definition of divergence operator

We now detail the definition of the discrete operator D_h and its adjoint D_h^*, developed to increase the efficiency for the computation of the volumetric contribution. When

considering the computation of the pressure term at the discrete level, we can write

$$\begin{aligned}\int_\Omega q_h \ \mathrm{div}\,\underline{w}_h \,\mathrm{d}\Omega &= \sum_{K\in\mathcal{T}_h}\int_K q_h \ \mathrm{div}\,\underline{w}_h \mathrm{d}K \\ &= \sum_{K\in\mathcal{T}_h}\int_{\widehat{K}} \widehat{q}_h \ \mathrm{div}(J_K \ \underline{\underline{\nabla}}\underline{\phi}_K^{-1} \ \widehat{\underline{w}}_h)\mathrm{d}\widehat{K} \\ &= \sum_{K\in\mathcal{T}_h}\int_{\widehat{K}} \widehat{q}_h \ \mathrm{cof}(\underline{\underline{\nabla}}\underline{\phi}_K) : \underline{\underline{\nabla}}\widehat{\underline{w}}_h \,\mathrm{d}\widehat{K}\end{aligned} \tag{34}$$

where

$$J_K = \det \underline{\underline{\nabla}}\underline{\phi}_K \quad \text{and} \quad \mathrm{cof}(\underline{\underline{\nabla}}\underline{\phi}_K) = J_K \ \underline{\underline{\nabla}}\underline{\phi}_K^{-T} \ .$$

Then, we have the displacement $\widehat{\underline{w}}_h$ and pressure $\widehat{q}_h$ w.r.t the reference element $\widehat{K}$. The computation performed on the element $\widehat{K}$ is a classical procedure in finite-element analysis as it allows simplifying and reducing computations. The last line of (34) can be rewritten with the application of the *Green's formula*, and we obtain

$$\int_\Omega q_h \ \mathrm{div}\,\underline{w}_h \,\mathrm{d}\Omega = -\sum_{K\in\mathcal{T}_h}\int_{\hat{K}} \mathrm{cof}(\underline{\underline{\nabla}}\underline{\phi}_K)\cdot\underline{\underline{\nabla}}\ \widehat{q}_h\cdot\widehat{\underline{w}}_h \,\mathrm{d}\widehat{\Omega}_K + \sum_{K\in\mathcal{T}_h}\int_{\partial\hat{K}} \mathrm{cof}(\underline{\underline{\nabla}}\underline{\phi}_K)\widehat{q}_h \ \widehat{\underline{w}}_h\cdot\hat{n}\,\mathrm{d}\hat{s} \tag{35}$$

On this reformulation we base the definition of discrete operators D_h and D_h^*, given by the application of a quadrature formula (Gauss Lobatto), to compute the integrals, so that we have

$$\begin{aligned}(D_h\underline{w}_h,q_h)_{\mathcal{L}} &:= (\underline{w}_h, D_h^* q_h)_{\mathcal{H}} \\ &:= -\sum_{K\in\mathcal{T}_h}\oint_{\hat{K}} \mathrm{cof}(\underline{\underline{\nabla}}\underline{\phi}_K)\cdot\underline{\underline{\nabla}}\widehat{q}_h\cdot\widehat{\underline{w}}_h \,\mathrm{d}\widehat{\Omega}_K + \sum_{K\in\mathcal{T}_h}\oint_{\partial\hat{K}} \mathrm{cof}(\underline{\underline{\nabla}}\underline{\phi}_K)\widehat{q}_h \ \widehat{\underline{w}}_h\cdot\hat{n}\,\mathrm{d}\hat{s}\end{aligned} \tag{36}$$

For the computation of the volumetric term we use a quadrature based on $(n+1)^d$ Gauss-Lobatto points. Moreover, we use a quadrature based on $(n+1)^{d-1}$ Gauss-Lobatto points on each facet of the reference element (4 when $d=2$, 6 when $d=3$).

An alternative would be to introduce $\widetilde{D}_h$ and $\widetilde{D}_h^*$ by

$$(\widetilde{D}_h\underline{w}_h, q_h)_{\mathcal{L}} := (\underline{w}_h, \widetilde{D}_h^* q_h)_{\mathcal{H}} := \sum_{K\in\mathcal{T}_h}\oint_{\widehat{K}} \widehat{q}_h \ \mathrm{cof}(\underline{\underline{\nabla}}\underline{\phi}_K) : \underline{\underline{\nabla}}\widehat{\underline{w}}_h \,\mathrm{d}\widehat{K} \tag{37}$$

using a quadrature based on $(n+1)^d$ Gauss-Lobatto points.

We now compare the computational cost associated to the application of $\widetilde{D}_h$ or D_h. The application of the operator $\widetilde{D}_h$ implies the computation of 9 derivatives for the gradient of the displacement field, plus the interpolation of the pressure field into $\mathcal{Q}_n$. The use of the proposed operator D_h, instead, requires the computation of 3 derivatives of the $\mathcal{Q}_{n-2}$ pressure field, 3 interpolations for the resulting gradient, and the computation of the boundary term that has a lower complexity. Without going into details our computations show that asymptotically, using D_h over $\widetilde{D}_h$ offers a reduction of 40% in terms of computational cost. Nevertheless, higher efficiency is expected for some specific choice of n as we explain in the following section.

3.2.4 The $\mathcal{Q}_4 - \mathcal{Q}_2^{disc}$ element

In practice to further increase the efficiency of the numerical scheme, we use for the order of $\mathcal{V}_h$ and $\mathcal{L}_h$ the couple spaces such that the DoFs of the pressure element correspond to a subset of the DoFs of the displacement element. By taking $n = 4$, we have the highest element order with the mentioned feature, reducing the number of operations for the interpolation from $\mathcal{L}_h$ to $\mathcal{V}_h$.

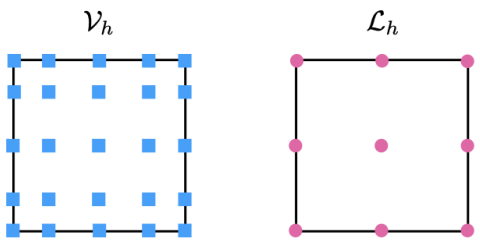

Figure 2. Representation of spectral elements choice with related DoFs distribution. From the left, $\mathcal{Q}_4(\hat{K})$ element of displacement space $\mathcal{V}_h$ and $\mathcal{Q}_2^{disc}(\hat{K})$ element for pressure space $\mathcal{L}_h$.

The computation is performed within a home-made software and the interpolation of the pressure field is specifically optimized in order to further speed up the computations. In our implementaton, no matrix is assembled since all the computations are done locally, which allow to strongly reduce the CPU storage and cost. We measure numerically a speed-up of 70% for the computation of the pressure contribution compared to the use of (37).

3.3 Time discretization

3.3.1 The leap-frog method

We now develop a fully-discretized scheme associated to the mixed formulation (NIMd). Given the time interval $[0, T]$, with $T > 0$, we define the partition $t^n = n\Delta t$, with $n \in \{0, 1, ...N\}$ and the time-step defined as $\Delta t = T/N$, we can introduce a time-discretization based on Leap-Frog method

$$M_h \frac{\underline{u}_h^{n+1} - 2\underline{u}_h^n + \underline{u}_h^{n-1}}{\Delta t^2} + (A_h^s + \lambda \bar{A}_h^p)\underline{u}_h^n = \underline{f}_h^n \qquad \text{in } \mathcal{V}_h \tag{LF}$$

The LF method is characterized by second order accuracy and energy conservation. It is fully explicit, which makes it useful to deal with large scale problem such as elastodynamic problems. However, the scheme is stable under the well-known CFL condition [**joly2007numerical**]

$$0 \leq \Delta t^2 A_h^s + \Delta t^2 \lambda \bar{A}_h^p \leq 4M_h \quad \Longleftrightarrow \quad \Delta t^2 \leq \frac{4}{\rho(M_h^{-1} A_h^s + \lambda\, M_h^{-1} \bar{A}_h^p)}, \tag{38}$$

where here $\rho(\cdot)$ now denotes the spectral radius of an operator. The enforcement of nearly-incompressibility corresponds to a large value of the bulk modulus λ. As a result, the maximal time-step to guarantee the stability of the scheme is strongly reduced, the number of iterations N to reach the end of the simulation at time T will proportionally increase.

For a physical interpretation, we could consider that with a large bulk modulus, the speed of pressure waves is much larger than shear waves (respectively $1500 ms^{-1}$

and $10ms^{-1}$ in biological tissues) and our explicit scheme should have a time step adapted to the the fastest wave propagation phenomena. Then, the pressure wave strongly limits the time-step and affects the efficiency of the computations.

3.3.2 Stabilised leapfrog method

As mentionned, the pressure operator $\lambda \bar{A}_h^p$ limits the time-step Δt, but at the same time it has a low computational cost, thanks to the proposed operators D_h and D_h^*. On the other side, the shear operator A^s has a lower spectral radius, around two order of magnitudes smaller compared to $\lambda \bar{A}_h^p$ in soft tissues, but it has a higher computational cost as it involves the computation of the gradient of displacements and accounts for all the complexities of the material (typically heterogeneities and anistropy). In this framework, we would like to separate the computation of shear and pressure wave operator. The shear waves is computed at a "global" larger time step, whereas pressure wave operator is computed as if "local" time-step were defined. This general idea is the basis of the Chebyshev Leapfrog method [**Carle2020**], such that at each time-step the shear part is iterated only once and the volumetric operator is iterated $m+1$ times.

In order to use the strategy suggested above, the pressure operator is approximated with a polynomial $\mathscr{P}_m(x)$ of order m, given the condition $\mathscr{P}_m(0) = 1$ to be consistent with the leap-frog scheme,

$$M_h \frac{\underline{u}_h^{n+1} - 2\underline{u}_h^n + \underline{u}_h^{n-1}}{\Delta t^2} + A^s \underline{u}_h^n + \mathscr{P}_m(\Delta t^2 \lambda \bar{A}_h^p M_h^{-1}) \lambda \bar{A}_h^p \underline{u}_h^n = \underline{f}_h^n. \tag{39}$$

We rewrite the stability condition (38) for our modified scheme

$$0 \leq \Delta t^2 A_h^s + \Delta t^2 \mathscr{P}_m(\Delta t^2 \lambda \bar{A}_h^p M_h^{-1}) \lambda \bar{A}_h^p \leq 4 M_h \tag{40}$$

from which we derive the following theorem for a polynomial $\mathscr{P}_m$ yet unspecified

Theorem 3.1. *A sufficient condition for the stability of the scheme* (39) *is*

$$\Delta t^2 \leq \frac{1}{\rho(M_h^{-1} A_h^s)} \tag{41}$$

and

$$\mathscr{P}_m(x) x \in [0,3] \quad \forall x \in [0, \rho(\Delta t^2 \lambda M_h^{-1} \bar{A}_h^p)] \tag{42}$$

Proof. From the stability condition of the modified scheme (40), we derive a sufficient condition

$$\begin{cases} \Delta t^2 A_h^s \leq M_h \\ \\ 0 \leq \Delta t^2 \mathscr{P}_m(\Delta t^2 \lambda \bar{A}_h^p M_h^{-1}) \lambda \bar{A}_h^p \leq 3 M_h. \end{cases} \tag{43}$$

The first condition (41) is then trivially obtained. Given that the pressure operators is self-adjoint and positive, we can then apply the Spectral Mapping theorem [**Harte1972**] to reduce the analysis to a spectral analysis. More precisely, for condition (42), we see that the second equation of (43) can be written in terms of the spectrum σ

$$\sigma\left(\Delta t^2 M_h^{-1} \mathscr{P}_m(\Delta t^2 \lambda \ \bar{A}_h^p M_h^{-1}) \lambda \ \bar{A}_h^p \right) \in [0,3]$$

which is equivalent to

$$\sigma\Big(\mathscr{P}_m(\Delta t^2\lambda\, M_h^{-1}\bar{A}_h^p)\Delta t^2\lambda\, M_h^{-1}\bar{A}_h^p\Big) \in [0,3]$$

Hence, the spectrum les in $[0,3]$ if the polynomial $\mathscr{P}_m$ is such that

$$\mathscr{P}_m(x)x \in [0,3] \quad \forall x \in [0, \rho(\Delta t^2 \lambda M_h^{-1}\bar{A}_h^p)] \tag{44}$$

concluding the proof. □

Notice that the implementation of the polynomial $\mathscr{P}_m$ should be obtained with an algorithm, for example like the Horner's rule or recurrance rules, so that the computation of the volumetric contribution of the displacement would correspond to the application of the argument of the polynomial for $m+1$ times.

3.3.3 Leapfrog Chebyschev Methods

First note that – following (41) – the time step Δt is chosen independently of the choice of $\mathscr{P}_m$. We set

$$\Delta t = (1-\epsilon)\frac{1}{\sqrt{\rho(M_h^{-1}A_h^s)}} \qquad \text{with} \quad \epsilon \ll 1. \tag{45}$$

For the choice of the polynomial, we use the so-called *stabilized* or *damped Chebyshev Polynomials* $\mathscr{P}_m^\nu$, proposed by [**Carle2020**], and obtained from scaling and shifting of Chebyshev polynomials of first kind $\mathscr{T}_m(x)$:

$$\mathscr{P}_m^\nu(x) = \frac{2}{x}\left[1 - \frac{\mathscr{T}_{m+1}(\delta_m^\nu - \frac{x}{\omega_m^\nu})}{\mathscr{T}_{m+1}(\delta_m^\nu)}\right] \tag{46}$$

with parameters δ_m^ν and ω_m^ν

$$\delta_m^\nu = 1 + \frac{\nu}{(m+1)^2}, \qquad \omega_m^\nu = 2\frac{\mathscr{T}'_{m+1}(\delta_m^\nu)}{\mathscr{T}_m(\delta_m^\nu)},$$

and first order derivative $\mathscr{T}'_{m+1}(x) = (m+1)\mathscr{U}_m(x)$ where $\mathscr{U}_m$ is the Chebyshev of second kind. We see that consistency with respect to the original scheme is guaranteed, since

$$\mathscr{P}_m^\nu(x)x = 2\left[1 - \frac{\mathscr{T}_{m+1}(\delta_m^\nu - \frac{x}{\omega_m^\nu})}{\mathscr{T}_{m+1}(\delta_m^\nu)}\right] = x + \mathcal{O}(x^2) \tag{47}$$

and the Leap-Frog-Chebyshev scheme reads

$$M_h\frac{\underline{u}_h^{n+1} - 2\underline{u}_h^n + \underline{u}_h^{n-1}}{\Delta t^2} + A_h^s\underline{u}_h^n + \mathscr{P}_m^\nu(\Delta t^2\lambda\bar{A}_h^p M_h^{-1})\lambda\bar{A}_h^p\underline{u}_h^n = \underline{f}_h^n \tag{LFC}$$

Chebyshev polynomials are sequences of polynomial functions that can be computed with recurrence relations and benefit of optimal properties for the uniform distribution of its roots within the interval $[-1,1]$. The formulation (46) allows to change the interval in which Chebyshev polynomials oscillates, with the following properties derived in [**Carle2020**, **Grote2021**].

Property 3.1. *For $\nu \in [0,1]$:*

$$\sup_{x\in[0,\alpha_m]} |x\mathscr{P}_m^\nu(x)| < 4 - \frac{2\nu}{1+\nu} \qquad \textit{with} \qquad \alpha_m = \left(2 + \frac{\nu}{(m+1)^2}\right)\omega_m^\nu \tag{48}$$

and $\forall \beta \leq \alpha_m$

$$\inf_{x\in[\beta,\alpha_m]} |x\mathscr{P}_m^\nu(x)| > \min\left(\frac{\beta}{1+\nu}, \frac{2\nu}{1+\nu}\right) \tag{49}$$

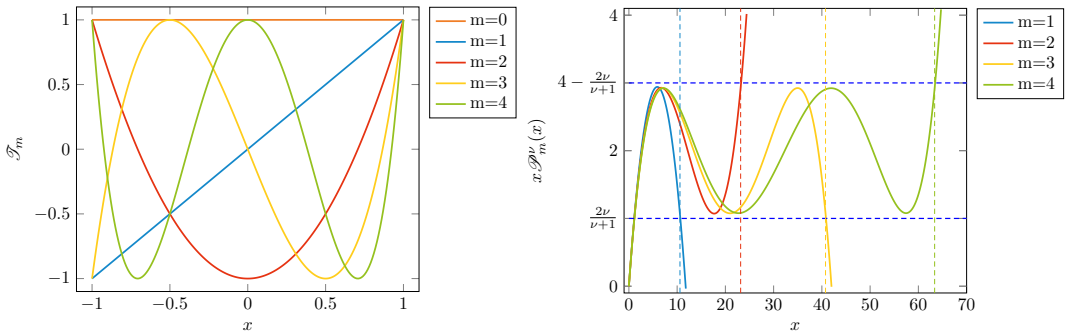

Figure 3. On the left: Chebyshev Polynomials of first kind with order m from 0 to 4. On the right: Stabilized Chebyshev polynomials $x\mathscr{P}_m^\nu$ with order m from 1 to 4. Dashed vertical lines correspond to α_m which guarantees that for $x \in [0, \alpha_m]$ we have $x\mathscr{P}_m^\nu < 4 - \frac{2\nu}{1+\nu}$. In the figure, $\nu = 1$.

This choice of polynomials allows to have the largest stability region (in x) in which the Chebyshev $x\mathscr{P}_m^\nu(x)$ is comprised between the inferior and the superior limit, as given by Property 3.1.

We now present the constructed solution in order to respect the sufficient condition of Theorem 3.1. There are two parameters to choose: the parameter ν that defines the inferior and superior limit of $\mathscr{P}_m^\nu$, and the polynomial order m that depends on the spectral radius of the pressure operator through the parameter α_m.

By taking $\nu = 1$, we define the superior limit of the polynomial within the stability region $[0, \alpha_m]$.

$$\sup_{x\in[0,\alpha_m]} |x\mathscr{P}_m^1(x)| < 3 \tag{50}$$

which partially corresponds to the second condition (42) of the stability condition of theorem 3.1.

Still, we remark that the stabilised Chebyshev polynomial is characterized by a superior limit only within the stability region $x \in [0, \alpha_m]$, for which we have to ensure that

$$\sigma(\Delta t^2 \lambda M_h^{-1} \bar{A}_h^p) \in [0, \alpha_m] \tag{51}$$

in order to guarantee condition (42). Since the positivity of the spectrum is given, we only need to respect

$$\rho(\Delta t^2 \lambda M_h^{-1} \bar{A}_h^p) \leq \alpha_m \tag{52}$$

From an estimation of α_m, we see that for $\nu > 0.7$ we have

$$4(m+1)^2 e^{-\nu/2} \leq \alpha_m$$

By substitution, we derive the minimum order of the damped Chebyshev polynomial

$$m+1 \geq \sqrt{\lambda}\frac{\sqrt{\rho(\Delta t^2 M_h^{-1}\bar{A}_h^p)}e^{1/4}}{2}\,. \tag{53}$$

To sum up, the stability of the scheme (LFC) is given by the following proposition

Proposition 3.2. *A sufficient condition to guarantee the stability of the Leapfrog Chebyshev scheme* (LFC) *is given by*

Maximum time step

$$\Delta t \leq (1-\epsilon)\frac{1}{\sqrt{\rho(M_h^{-1}A_h^s)}} \qquad \textit{with} \quad \epsilon \ll 1 \tag{54}$$

Minimum order of polynomial $x\mathscr{P}_m^1(x)$

$$m+1 = \left\lceil \sqrt{\lambda}\frac{\sqrt{\rho(\Delta t^2 M_h^{-1}\bar{A}_h^p)}e^{1/4}}{2} \right\rceil \tag{55}$$

Note that in Proposition 3.2 the operator $\lceil\cdot\rceil$ outputs the smallest larger integer. With the introduction of polynomial $\mathscr{R}_{m+1}(x) := x\mathscr{P}_m^1(x)$, the fully-discretized scheme reads

$$\underline{u}_h^{n+1} - 2\underline{u}_h^n + \underline{u}_h^n + \Delta t^2 M_h^{-1}A_h^s\underline{u}_h^n + \mathscr{R}_{m+1}(\Delta t^2\lambda M_h^{-1}\bar{A}_h^p)\underline{u}_h^n = \Delta t^2 M_h^{-1}\underline{f}^n \tag{LFC}$$

In conclusion, we have developed a stable explicit scheme for linear elastic wave propagation in incompressible media. The stability of the scheme is based on the definition of a time step Δt from the shear operator only and on the order of a stabilised Chebyshev polynomials. One way to interpret this is to say that the *global* time step Δt is chosen using the shear operator only, while the pressure terms are computed with a *local* time-step $\Delta t_m = \Delta t/(m+1)$. As we will see in the Results section, the efficiency of the scheme w.r.t. the LF method relies on two points: First, the low computational cost of the pressure operator compared to the shear operator ; Second, the value of λ, the higher λ is, higher will be the potential gain given by this strategy.

The implemented algorithm for computing the solution to (LFC) is given Algorithm 1. It is based on the recurrence relations of the Chebyshev polynomials. An auxiliary variable $\underline{z}_l^n$ is introduced, with $l = 0, ..., m+1$, which corresponds to the *local* contribution of the pressure operator within each time step n.

3.4 Efficiency estimation the LFC scheme

Let us now present a theoretical estimation of the computational gain that we obtain with the (LFC) scheme w.r.t. to the classical Leap-Frog scheme (LF).

We denote C_S the computational time for the application of the shear operator, and C_P the computational time for the application of the pressure operator. The objective is to compare the simulation time of the LF method and of the LFC method, based on C_S and C_P and on the time-steps Δt_{LF} and Δt_{LFC} derived from the respective stability condition. The quantity that we would like to analyze is the computational

Algorithm 1 Algorithm for the (LFC) scheme

$\underline{z}_0^n \leftarrow \underline{u}_h^n$

$\underline{z}_1^n \leftarrow \delta_m^1 \underline{u}_h^n - \dfrac{\Delta t^2 \lambda}{\omega_m^1} M_h^{-1} \bar{A}_h^p \underline{u}_h^n$

for $l = 2 : m+1$ **do**

$\underline{z}_l^n \leftarrow 2\left(\delta_m^1 I - \dfrac{\lambda \Delta t^2}{\omega_m^1} M_h^{-1} \bar{A}_h^p\right) \underline{z}_{l-1}^n - \underline{z}_{l-2}$

end for

$\mathscr{R}_{m+1}(\Delta t^2 \lambda M^{-1} \bar{A}_h^p) \underline{u}_h^n \leftarrow 2\underline{u}_h^n - \dfrac{2\underline{z}_{m+1}^n}{\mathscr{T}_{m+1}(\delta_m^1)}$

$\underline{u}_h^{n+1} \leftarrow \Delta t^2 M_h^{-1} \underline{f}^n - \underline{u}_h^{n-1} + 2\underline{u}_h^n - \Delta t^2 M_h^{-1} A_h^s \underline{u}_h^n - \mathscr{R}_{m+1}(\Delta t^2 \lambda M^{-1} \bar{A}_h^p) \underline{u}_h^n$

gain G defined as follows

$$G = \frac{N_{LF} C_{LF}}{N_{CH} C_{LFC}}$$

where N_{LF} and N_{LFC} are the number of iterations to complete a simulation, while C_{LF} and C_{LFC} are the computational cost of the time step for each method.

We start from the classic LF scheme considering that, with the property that the shear and pressure operators are positive and self-adjoint, we have

$$\rho(M_h^{-1} A_h^s + \lambda\, M_h^{-1} \bar{A}_h^p) \leq \rho(M_h^{-1} A_h^s) + \rho(\lambda\, M_h^{-1} \bar{A}_h^p) \tag{56}$$

Then, the CFL condition (38) is respected for the following time-step

$$\Delta t_{LF}^2 = \frac{4}{\rho(M_h^{-1} A_h^s) + \rho(\lambda\, M_h^{-1} \bar{A}_h^p)} = \rho(M_h^{-1} A_h^s) \frac{4}{1 + \lambda R} \qquad R := \frac{\rho(M_h^{-1} \bar{A}_h^p)}{\rho(M_h^{-1} A_h^s)}. \tag{57}$$

The choice of time step given by (57) may appear suboptimal because (56) is in general a strict inequality. However for large λ the difference between, $\rho(M_h^{-1} A_h^s + \lambda\, M_h^{-1} \bar{A}_h^p)$ and the sum of the spectral radii is small with respect to λ. The computational time of a single time step in the LF scheme is trivially given by

$$C_{LF} = C_S + C_P\ . \tag{58}$$

For the LFC scheme, we have constructed the stability condition by choosing

$$\Delta t_{LFC}^2 = \frac{1}{\rho(M_h^{-1} A_h^s)}\ . \tag{59}$$

Notice that with respect to the time-step defined in (45), we forget the term $(1 - \epsilon)$ for the sake of simplicity. For the evaluation of the computational cost of a time-step with the LFC method, we have

$$C_{LFC} = C_S + (m+1) C_P$$

where we take $m+1$ as the minimal value to guarantee the stability condition (53), and we combine with (59) in order to obtain

$$C_{LFC} = C_S + \left\lceil \Delta t_{LFC} \frac{\sqrt{\lambda\rho(M_h^{-1}\bar{A}_h^p)}e^{1/4}}{2} \right\rceil C_P = C_S + \left\lceil \frac{e^{1/4}}{2}\sqrt{\lambda R}\, C_P \right\rceil .$$

Now that we have all the elements, we rewrite the computational gain G as

$$G = \frac{\frac{1}{\Delta t_{LF}} C_{LF}}{\frac{1}{\Delta t_{LFC}} C_{LFC}} = \frac{\Delta t_{LFC} C_{LF}}{\Delta t_{LF} C_{LFC}}$$

We notice that we can write the ratio between Δt_{LFC} and Δt_{LF} as a function of the quantity R from relations (57) and (59)

$$\frac{\Delta t_{LFC}}{\Delta t_{LF}} = \frac{\sqrt{1+\lambda R}}{2}$$

Finally, the computational gain G is given by the following relation

$$G = \frac{\sqrt{1+\lambda R}}{2} \frac{C_S + C_P}{C_S + \left\lceil \frac{e^{1/4}}{2}\sqrt{\lambda R}\, C_P \right\rceil} \tag{60}$$

Considering the incompressible limit ($\lambda \to \infty$), we have

$$\lim_{\lambda\to\infty} G = \frac{\sqrt{\lambda R}}{2} \frac{C_S + C_P}{\frac{e^{1/4}}{2}\sqrt{\lambda R}\, C_P} = e^{-1/4}\left(\frac{C_S}{C_P} + 1\right)$$

for which we obtain that the LFC scheme is more efficient than the LF scheme (i.e. $G > 1$) if the computational cost of the pressure operator is sufficiently smaller that the shear operator, in particular

$$C_S/C_P > e^{1/4} - 1 \approx 0.2840 \, . \tag{61}$$

In practice, this condition is always met, for which we show that at the incompressible limit the proposed (LFC) scheme is more efficient than the (LF).

In addition, we point out that the strategy developed for the space discretization Section 3.2 has an impact also on the efficiency estimation that we have propose by G. Indeed, the optimization for the computation of the pressure contribution corresponds to a decrease the computational cost for the pressure operator C_P, i.e. a higher efficiency of the scheme through relation (61), given that C_S is the same.

4 Numerical Results

This section is devoted to the presentation of numerical results in order to validate the properties of the proposed scheme (LFC). Before presenting details of the simulations, we consider the non-dimensionalization of the wave propagation problem. As in [**Caforio2018**], we introduce the characteristic length L of the domain Ω, the characteristic observation time T and the shear parameter μ. The non-dimensionalized displacement and pressure field reads respectively:

$$\underline{u}_a(t_a, \underline{x}_a) := L^{-1}\underline{u}(Tt_a, L\underline{x}_a) \qquad \text{and} \qquad p_c(t_a, \underline{x}_a) := \mu^{-1}p(Tt_a, L\underline{x}_a)$$

with $t_a \in [0,1]$. We then derive the non-dimensionalized quantities

$$\varrho_a = \frac{L^2 \varrho}{T^2 \mu}, \qquad \mathbf{C}_a^d = \mu^{-1} \mathbf{C}^d, \qquad \lambda_a = \frac{\lambda}{\mu}, \qquad \underline{f}_a = \frac{L}{\mu} \underline{f}$$

and with these, we rewrite our wave propagation problem in a non-dimensional form. For the rest of the paper, we drop the notation $(\cdot)_a$ that represents non-dimensionalized quantities.

In the following results, the source term used to generate the wave propagation has always the same form. It is the product of a spatial and a temporal term. The spatial excitation is a C^∞ function with a compact support, localized in the center of our solid $\underline{x}_C$. For the temporal push, we have a Ricker wavelet with a small offset t_0. The source term reads:

$$f(\underline{x}, t) = \begin{cases} A_m \cdot \exp\left[\frac{1}{2\sigma_s}\left(\frac{r_0^2}{d^2 - r_0^2} + 1\right)\right] \cdot \left[\left(\frac{t-t_0}{\sigma_\tau}\right)^2 - \frac{1}{\sigma_\tau}\right] \exp\left[-\frac{(t-t_0)^2}{\sigma_\tau}\right] & \text{if } d^2 < r_0^2 \\ 0 & \text{otherwise} \end{cases} \tag{62}$$

with $d^2 = \sum_{i=1}^{dim} (x_i - x_{C,i})^2$ with d the distance from the center, r_0 the maximum width of the source, A_m the maximum amplitude, σ_τ and σ_s the covariance.

4.1 Non-locking mixed formulation

We compare simulation results of the nearly-incompressible wave propagation problem considering the two semi-discretized schemes (NId) and (NIMd) respectively obtained with the displacement-based and mixed method. At this point we do not use the strategy developed with Chebyshev polynomials and we use the classic LF scheme for the time discretization.

Let us now provide numerical and physical parameters of simulations. We consider a 2D circular domain with non-dimensionalized density $\varrho = 1$. We consider isotropic homogeneous behavior, characterized by the constitutive relation (non-dimensionalized)

$$\underline{\underline{\sigma}} = 2\,\underline{\underline{\varepsilon}}(\underline{u}) + \lambda\,\mathrm{tr}(\underline{\underline{\varepsilon}}(\underline{u})). \tag{63}$$

We choose the non-dimensionalized second Lamé parameters as $\lambda = 2000$. The function described in (62) is used with $\underline{x}_C = (0,0)$. A vector field is generate by assuming that the source is polarized in the y-direction: $\underline{f} = f\underline{e}_y$. The other chosen parameters of the source are: $A_m = 10^6$, $r_0 = 0.05$, $\sigma_s = 0.5$, $\sigma_\tau = 2.5 \cdot 10^{-4}$.

For the space discretization, we compare the two schemes by using $\mathcal{Q}_4$ elements for the displacement-based method (NId), while for the mixed method we discretize with $\mathcal{Q}_4 - \mathcal{Q}_2^{disc}$ elements, as presented in (30) and (31). In both cases the mesh is highly refined, with 150k DoFs.

In figure 4 we have the magnitude of the displacement field obtained from the mixed method, in which we can appreciate only the propagation of the shear wave. In an isotropic homogeneous material the velocity of propagation of shear wave (v_s) and of pressure wave (v_p) are related to the material parameters such that

$$v_s^2 = \frac{\mu}{\varrho}, \qquad v_p^2 = \frac{\lambda + 2\mu}{\varrho}$$

With the present choice of material parameters, we have that $v_p \approx 45\ v_s$. Then, when looking at the resulting displacement field, we only see a propagating shear wave and

not the pressure one (in figure 4), as the pressure is too fast for the present timescale. We show the displacement results only of the mixed method (NIMd), as no qualitative difference is present with respect to the solution of the displacement-based method.

Then, we extract the volumetric component from the solution (which corresponds to $\lambda \nabla \mathrm{div}\, \underline{u}$) a posteriori, by computing the quantity

$$-\frac{\underline{u}_h^{n+1} - 2\underline{u}_h^n + \underline{u}_h^{n-1}}{\Delta t^2} - M_h^{-1} A_h^s \underline{u}_h^n$$

for both displacement-based and mixed method. The limitations of the displacement-based method previously mentioned is visible. In figure 5 we observe nonphysical oscillations in the pressure field that propagates with the shear wave, which is a numerical effect due to enforcement of incompressibility. This phenomenon disappears with the implemented mixed method, as we can see from figure 6.

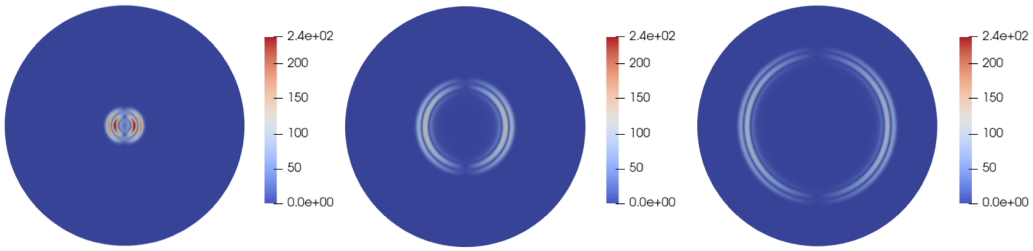

Figure 4. Elastic wave propagation in homogeneous isotropic solid. Magnitude of displacement field obtained with the mixed scheme. The 2D circular mesh is discretized with 150k Dofs.

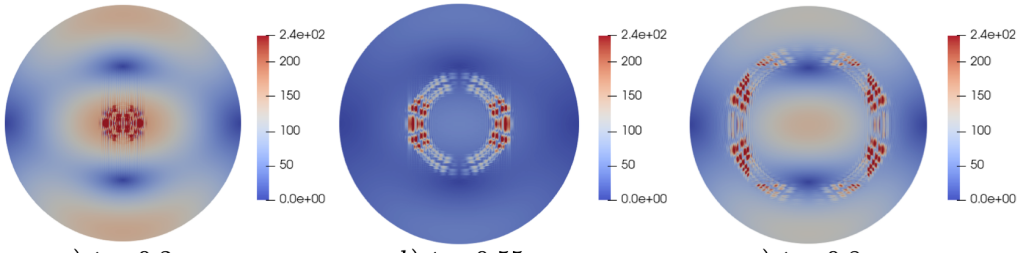

Figure 5. Volumetric component of the elastic wave propagation in homogeneous isotropic solid, with incompressible parameter $\lambda = 2000$. The 2D circular mesh is discretized with 150k Dofs. Solution obtained with displacement based method (NId), characterized by the presence of nonphysical oscillations coupled with the shear wave

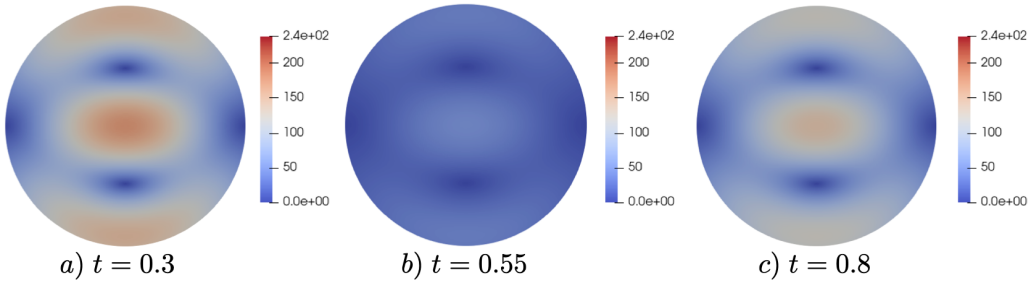

Figure 6. Volumetric component of the elastic wave propagation in homogeneous isotropic solid, with incompressible parameter $\lambda = 2000$. The 2D circular mesh is discretized with 150k Dofs. Solution obtained with displacement based method (NIMd). In this case, no spurious pressure wave is observed.

One important remark is that in this simulation we are far from the nearly-incompressible case. In biological tissues, the pressure wave has a velocity that is at least 2 orders of magnitude higher than the shear wave velocity. Yet, in our case we can already see the importance of approximating this type of problems with an appropriate mixed formulation. Nevertheless, these are well-known results when dealing with nearly-incompressible problems [**Bathe2006**, **brezzi2014basic**]. The primary objective of the space discretization strategy was to compute efficiently the pressure contribution, ensuring the stability of the method and the accuracy of the computation for both displacements and pressure.

4.2 Leapfrog Chebyschev Methods

4.2.1 Efficiency

We perform simulations of elastic wave propagation in isotropic homogeneous solids within different domains: square, circle and cube. For the material, we take $\varrho = 1$, $\lambda = 1000$ and the same parameters of the source that we have used in the previous section. In Table 1 we present the associated numerical results. We measure the simulation time η_{LF} and η_{LFC} with the LF and LFC scheme. The average computational cost of C_P and C_S is measured over 1000 iterations, and the ratio C_S/C_P can be then compared to the measured computational gain $G_{eff} = \eta_{LF}/\eta_{LFC}$. We underline that the effective computational gain G_{eff} is related to simulations with $\lambda = 1000$, while the estimated G corresponds to the limit case of incompressibility $\lambda \to \infty$. Yet, we see a significant gain in the order of 3 for 2D solid and in the order of 2 for 3D solid. We remark that a 3D simulation with $1,5$M of DoFs of elastic wave propagating within a nearly-incompressible isotropic homogeneous cube takes around 6 minutes.

In addition, the present case of study is given by an isotropic material linearized at rest condition, which is a very simplified case compared to possible realistic application. If we consider the biomedical application, tissues often undergoes large load and present anisotropic behavior. If we were supposed to model this type of problems, then the shear operator will be much more complex and the ratio C_S/C_P would be higher and so the computational gain G with respect to the classical LF method.

4.2.2 Space-time Convergence analysis

As a final validation of the proposed numerical scheme, we present a convergence analysis over space and time, comparing different boundary conditions. We consider a 2D square with $\Omega = [0, 1]^2$, discretized with N elements for each direction, from $N = 8$

Shape	η_{LF}[s]	η_{LFC}[s]	G_{eff}	C_S/C_P	$NDoF$
Square	12.24	5.23	2.34	1.99	51,842
Circle	41.82	14.76	2.83	2.77	154,242
Cube	799.0	377.18	2.12	1.76	1,594,323

Table 1. Numerical results of time efficiency of LF-Chebyshev Scheme w.r.t. to Leap-Frog scheme, considering different domains. η_{LF} and η_{LFC} are the measured simulation time for the computation of the elastic wave propagation in an isotropic homogeneous solid. G_eff is the effective computational gain measured.

to 256. The parameters of the source are the following: $A_m = 10^3$, $r_0 = 0.05$, $\sigma_s = 0.5$, $\sigma_\tau = 0.5 \cdot 10^{-4}$.

We compute the $\mathrm{L}^\infty(\mathrm{L}^2(\Omega))$ norm and the $\mathrm{L}^\infty(\mathrm{H}^1(\Omega))$ norm of the displacement error taking the LF scheme as a reference, and we plot it with respect to the space-step h. In these simulations we take $\lambda = 1000$. For each image, we consider the convergence of simulations with final times of simulation $T = 0.6$ and $T = 1.0$. In shorter simulations ($T = 0.6$) the shear wave almost reaches the boundary, but is not reflected, while with the longer simulations $T = 1.0$, we have reflection and possible effects of boundary conditions. Figure 7 represents the results obtained with a free boundary ($\underline{t} = 0$). Results show that second order convergence is maintained for both $\mathrm{L}^2(\Omega)$ and $\mathrm{H}^1(\Omega)$ norms (in space) for the shortest simulations ($T = 0.6$), (i.e. no reflection). With longer simulations ($T = 1.0$), we see instead a strong deterioration of convergence rate, which is not the same for the two norms: the order is two times smaller for $\mathrm{L}^2(\Omega)$ norm and four times smaller for $\mathrm{H}^1(\Omega)$.

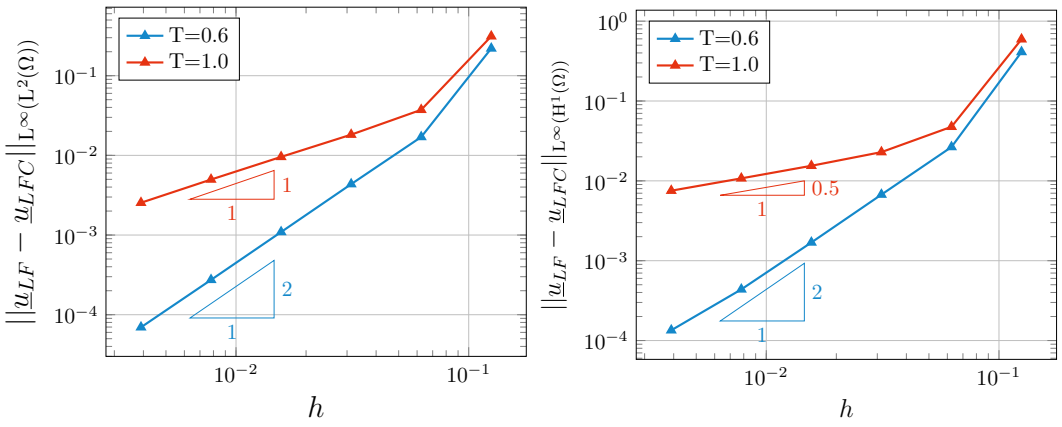

Figure 7. Convergence of scheme LFC with respect to the space step h – with $\underline{t} = 0$ on Γ (*free boundary condition*). On the left: we plot the $\mathrm{L}^\infty(\mathrm{L}^2(\Omega))$-displacement error for a final simulation time $T = 0.6$ (before the shear wave touches the boundary) and $T = 1.0$ (after reflection on the boundary). On the right we have an equivalent plot but with $\mathrm{L}^\infty(\mathrm{H}^1(\Omega))$-displacement error.

Then, we choose Dirichlet boundary condition $\underline{u} = 0$ on Γ, and we present the related convergence rate in figure 8. The simulations are obtained with the same material and source parameters as before. The convergence rate are now not affected by the boundary condition, as we see that no deterioration appears between simulations with different length in time. In addition, we see that the error is homogeneous between the two space norms $\mathrm{L}^2(\Omega)$ and $\mathrm{H}^1(\Omega)$, as expected. We point out that with Dirichlet

boundary condition, the proposed (LFC) scheme maintains the second order accuracy of the classical (LF) scheme.

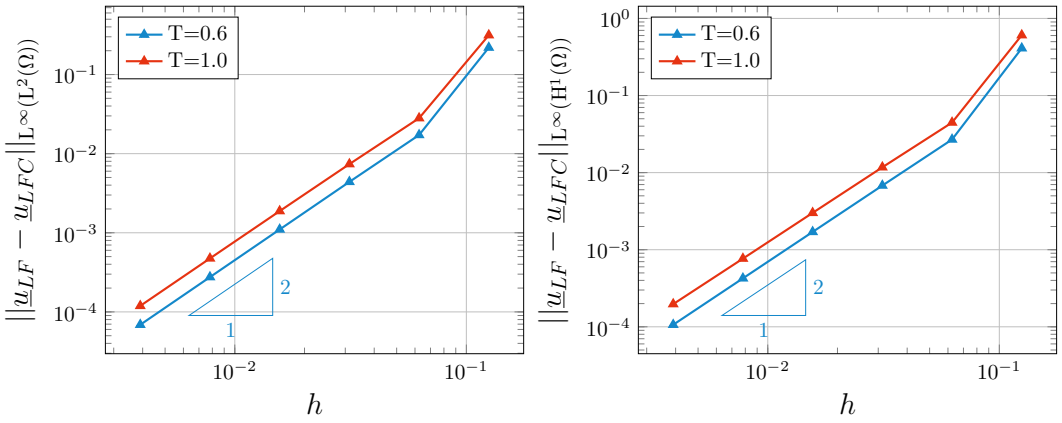

Figure 8. Convergence of scheme LFC with respect to the space step h – with $\underline{u} = 0$ on Γ (*Dirichlet boundary condition*). On the left, we plot the $L^\infty(L^2(\Omega))$ norm of displacement error. On the right, we plot the $L^\infty(H^1(\Omega))$ norm of the displacement error. In both case we consider a final simulation time $t_f = 0.5$ – before the shear wave touches the boundary – and $t_f = 1.0$ – after reflection on the boundary.

5 Numerical application: elastic wave propagation in an incompressible hyperelastic stretched cube

In the previous section, we presented the numerical scheme for wave propagation problem in nearly-incompressible isotropic solids linearized around at rest condition. We now want to present the applicability of the LFC scheme for the approximation of linear wave propagation problems within solids with large deformations. The formulation obtained in section 2 allows to give a physical interpretation of the wave propagation, depending on material and prestress effect.

In the following applications, the solution of the non-linear nearly-incompressible static problem is approximated by the solution of the of the pure incompressible problem (64) with a non-homogeneous Dirichlet boundary condition yet unspecified. We solve the following static non-linear problem :

Find $(\underline{u}_0, p_0) \in \mathcal{W} \times \mathcal{L}$ such that

$$\begin{cases} \displaystyle\int_{\widehat{\Omega}} \underline{\underline{\Sigma}}_0^d : \mathrm{D}\underline{\underline{e}}_0(\underline{\widehat{v}})\, \mathrm{d}\widehat{\Omega} - \int_{\widehat{\Omega}} p_0 J_0 \underline{\underline{C}}_0^{-1} : \mathrm{D}\underline{\underline{e}}_0(\underline{\widehat{v}})\, \mathrm{d}\widehat{\Omega} = 0 & \forall\, \underline{\widehat{v}} \in \mathcal{V}(\widehat{\Omega}) \\ \displaystyle\int_{\widehat{\Omega}} \widehat{\varrho}(J_0 - 1) \cdot q\, \mathrm{d}\widehat{\Omega} = 0 & \forall\, q \in \mathcal{L}(\widehat{\Omega}) \end{cases} \tag{64}$$

where p_0 is now a *Lagrangian multiplier*.

Let us consider a hyperelastic isotropic material with the Neo-Hookean elastic potential

$$\mathscr{W}^d = \mu(J_1 - 3) \qquad \text{with} \quad J_1 = I_1 I_3^{-\frac{1}{3}} \tag{65}$$

where J_1 is the first reduced invariant presented in (10), and $\mu \in \mathbb{R}^+$ is the material parameter. As presented in the previous section, we consider a non-dimensionalization of the problem with respect to a characteristic length L, an observation time T and the material parameter μ.

Solving the non-linear static problem will give us access to the deformed *apparent* configuration Ω_0 given by $\underline{u}_0$, the related state of stress characterized by $\underline{\underline{\sigma}}_0$ and the internal pressure p_0.

The wave propagation problem is then obtained by linearization around $(\underline{u}_0, p_0)$, with the introduction of a large penalizing constant $\lambda \in \mathbb{R}^+$

For any time $t \in [0,1]$, find $(\widetilde{\underline{u}}(t), \tilde{p}(t)) \in \mathcal{V} \times \mathcal{L}$ such that

$$\begin{cases} \displaystyle\int_{\Omega_0} \varrho_0 \, \partial_{tt}\widetilde{\underline{u}} \cdot \underline{v} \, \mathrm{d}\Omega_0 + \int_{\Omega_0} \zeta \, \underline{\underline{\varepsilon}}(\widetilde{\underline{u}}) : \underline{\underline{\varepsilon}}(\underline{v}) \, \mathrm{d}\Omega_0 \; + \int_{\Omega_0} \underline{\underline{\nabla}}_{x_0} \widetilde{\underline{u}} \, \underline{\underline{\sigma}}_0 : \underline{\underline{\nabla}}_{x_0} \underline{v} \\ \qquad\qquad + \displaystyle\int_{\Omega_0} \tilde{p} \, \mathrm{div}\, \underline{v} \, \mathrm{d}\Omega_0 = \int_{\Omega_0} \widetilde{\varrho_0 \underline{f}} \cdot \underline{v} \, \mathrm{d}\Omega_0 \qquad \forall \, \underline{v} \in \mathcal{V} \\ \displaystyle\int_{\Omega_0} q \, \mathrm{div}\, \widetilde{\underline{u}} \, \mathrm{d}\Omega_0 = \lambda^{-1} \int_{\Omega_0} \tilde{p} \, q \, \mathrm{d}\Omega_0 \qquad \forall \, q \in \mathcal{L} \end{cases} \tag{66}$$

with

$$\widetilde{\underline{u}}(t=0) = \partial_t \widetilde{\underline{u}}(t=0) = 0 \quad \text{in } \Omega_0$$

where the material tangent stiffness is now given by the scalar ζ, that depends on the loading condition of the non-linear static problem. Notice that the reduction of the material stiffness to a scalar ζ is related to our choice of the potential $\mathscr{W}^d$ in (65). For the following simulations, we will always take the penalizing parameter $\lambda = 1000$.

For the application of the scheme, we consider a simple example for the non-linear static case, such that the solution of problem (64) can be found analytically. In order to test the scheme and see the effects of the loaded state over the wave propagation, we take a homogeneous cube with a domain $\widehat{\Omega} = [0,1]^3$ and we choose a non-linear solid with isotropic homogeneous property as presented in (65).

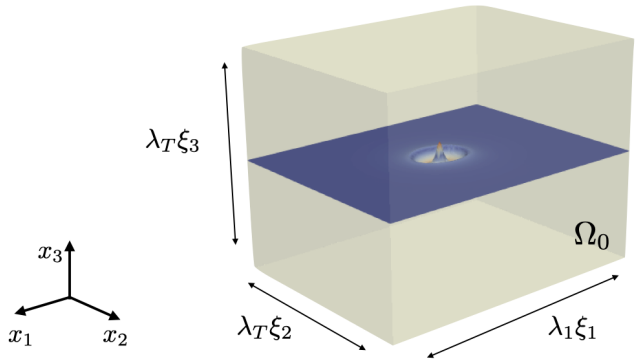

Figure 9. Examples of loaded configurations analyzed for the application of the numerical scheme

The solution is sought as a uniform stretch state given by λ_1, λ_2 and λ_3, which describe the stretch in the Cartesian coordinates. We have a deformation map $\underline{\phi}_0(\underline{\xi})$, that reads

$$\underline{\phi}_0(\underline{\xi}) = (\lambda_1 \xi_1, \, \lambda_2 \xi_2, \, \lambda_3 \xi_3)^T$$

with $\lambda_1 = \bar{\lambda}_1$ (given) and $\lambda_2 = \lambda_3 = 1/\sqrt{\bar{\lambda}_1}$ due to incompressibility.

The state of stress in the reference configuration is given by the following relation

$$\underline{\underline{\Sigma}}(\underline{u}, p) = \underline{\underline{\Sigma}}_d - pJ\underline{\underline{C}}^{-1} = \frac{\partial \mathscr{W}^d}{\partial \underline{\underline{e}}} - pJ\underline{\underline{C}}^{-1} \tag{67}$$

where the hydrostatic pressure p is now defined as a lagrangian multiplier. We can derive analytically the state of stress in the apparent configuration, taking into account that in the transverse direction there is no constraint. Then, the non-dimensionalized Cauchy tensor is in the form $\underline{\underline{\sigma}}_0 = \sigma_0\, \underline{e}_1 \otimes \underline{e}_1$ with

$$p_0 = -\frac{2}{3}\left(\bar{\lambda}_1^2 - \frac{1}{\bar{\lambda}_1}\right)$$
$$\sigma_0 = \frac{4}{3}\left(\bar{\lambda}_1^2 - \frac{1}{\bar{\lambda}_1}\right) - p_0 = 2\left(\bar{\lambda}_1^2 - \frac{1}{\bar{\lambda}_1}\right)$$

Once we have the solution of the non-linear static problem, we can derive the parameters for the wave propagation problem (66). The geometric stiffness is given by $\underline{\underline{\sigma}}_0$, while the material stiffness is obtained by linearization and it reduces to

$$\zeta = \frac{4}{3}\,\mathrm{tr}\,(\underline{\underline{C}}_0) + 2p_0 = \frac{4}{\bar{\lambda}_1} \tag{68}$$

From these preliminary results we can already observe that increasing the imposed stretch $\bar{\lambda}_1$ results in an increase of the geometric stiffness and a reduction of the material stiffness parameter ζ.

The volumetric transient source for the excitation of the wave is defined with the previous formula (62) and polarized in the $\underline{e}_3$-direction such that $\underline{f} = f(\underline{x}_0, t) \cdot \underline{e}_3$. The spatial excitation is localized in the center of the stretched cube. We take $r_0 = 0.05$, $\sigma_s = 10$ and $A_m = 5$. For the temporal push we have a Ricker wavelet with a small offset $t_0 = 0.04$ and $\sigma_\tau = 200$.

In figure 10, we see an example of propagation of the elastic wave within the incompressible cube. The mesh is discretized with 30 hexahedra in each direction, with $\mathcal{Q}_4 - \mathcal{Q}_2^{disc}$ elements and 5.3M DoFs. The average time to run these simulations in a normal machine with visual results is of 6 minutes.

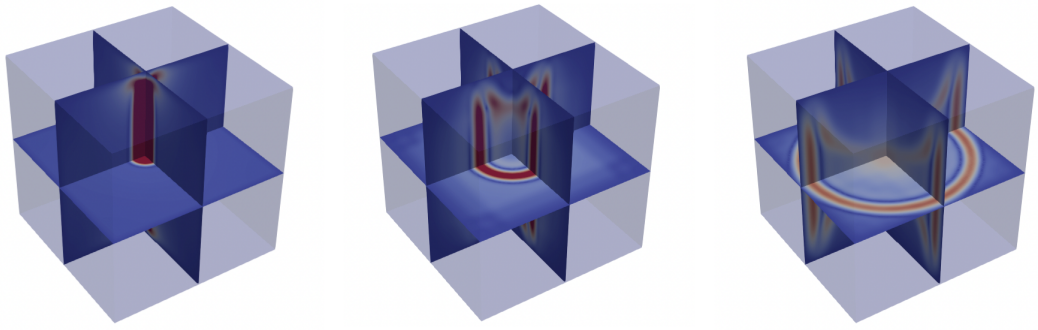

$t = 0.1$ $t = 0.3$ $t = 0.6$

Figure 10. Simulation of 3D elastic wave propagation within an incompressible isotropic cube. In the images we observe the propagation in time (from left to right) of the magnitude of the displacement field. The transient source is focalized in the center of the cube and polarized in the vertical direction. Magnitude displacement in [0.0, 0.1]

In order to see the effect of loaded configuration over the propagation of the wave, we consider three cases of stretch $\bar{\lambda}_1 = [1.0, 1.1, 1.2]$. In figure 11, we present results of wave propagation in the mid $x_1 - x_2$ plane of the cube. In the first case, where the cube has no pre-stretch, the wave propagates with a circular symmetric shape as the one given by the source. By increasing the static stretch $\bar{\lambda}_1$, we observe a deformation of the wave front, for which the wave is faster in the direction x_1 of the imposed stretch and slower in the perpendicular direction x_2 . As we noticed before, the material stiffness has actually decreased since the parameter ζ, related to the Neo-Hookean density function, is inversely proportional to the pre-stretch λ_1. As a consequence, a major role for the variation in the wave propagation is played by the geometric stiffness, which depends on the non-linear variation of strains and the pre-stress which has the only non-zero component in the $\underline{x}$ direction.

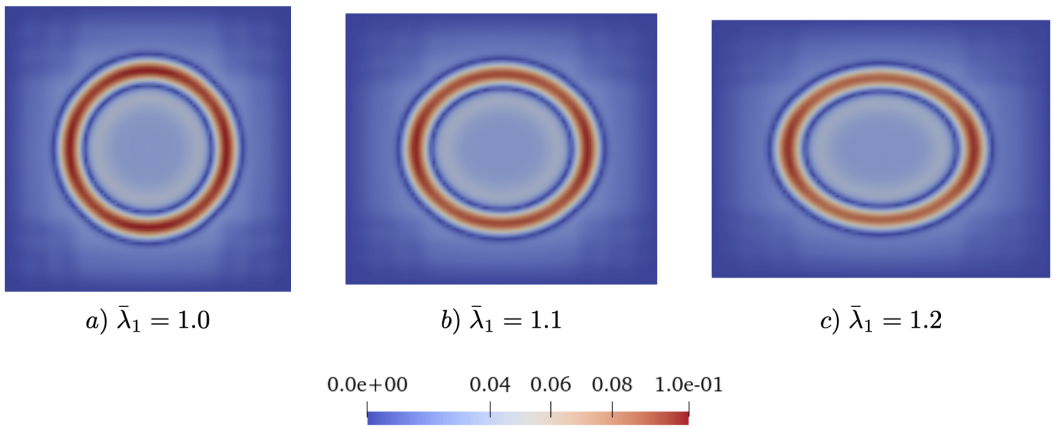

Figure 11. Increasing effect of pre-stretch over elastic wave propagation in nearly-incompressible cube with non-linear isotropic behavior subjected to uniaxial tension. Displacement magnitude in the middle $x_1 - x_2$ plane. From left $\bar{\lambda}_1 = [1.0, 1.1, 1.2]$. Mesh discretized with 5.3M DoFs. Wave observed at $t = 0.3$

To have a final validation of these results, we looked at the elastic wave propagation in the cube artificially turning off and on different terms of the problem, in order to compare the different effects. In figure 12(a) we show the reference case, wave propagation in the cube subjected to a prestretch $\bar{\lambda}_1 = 1.2$, which corresponds to the simulation previously discussed (figure 11(c)). Then, we consider (figure 12(b)) the wave propagation in a domain that corresponds to the one obtained from the non-linear static problem with $\bar{\lambda}_1 = 1.2$, but in the simulation we do not account for any pre-stretch effect on the material and geometric stiffness.The simulation in figure 12(c) show the wave propagation with *only the prestress effect* due to $\bar{\lambda}_1 = 1.2$, while we "turn off" the material stiffness term taking $\zeta = 4$. Finally, in figure 12(d), we have taken $\sigma_0 = 0$ and $\zeta = 4/\bar{\lambda}_1$ with $\bar{\lambda}_1 = 1.2$, which corresponds to a material behavior with the linearized material stiffness term and *no prestress* effect is considered.

The resulting displacement fields reflect what we expected by looking at the physical terms of our problem (66). When considering only the linearized material behavior (figure 12(d)), we see that the wave propagates homogeneously slower with respect the unloaded behavior given in (figure 12(a)). As mentioned before, the material stiffness parameter ζ is invertionally proportional to the pre-stretch (68), which has a visible

effect on the propagation of the shear wave. Obviously, this is related to the choice of the non-linear potential. The neo-hookean potential (65) presents a decreasing stiffness (slope) with the increasing loading condition, which corresponds to a softer response of the linearized material.

Still, the overall results that we have observed in figure 11 is an anisotropic response of the solid, with a relevant increase of the wave speed in the direction of the pre-stretch and a decrease in the perpendicular direction. As we can see in figure 12(c), the geometric stiffness (prestress) is the most relevant term in the propagation of the shear wave. Indeed, if we compare this result with the "real" solution of the pre-loaded wave propagation problem 12(a), the wave with only the geometric stiffness (c) actually propagates faster. Trivially, this result comes from the sum of the geometric effect with the material effect, where the latter tends to lower the stiffness of the material and so the speed of the wave front.

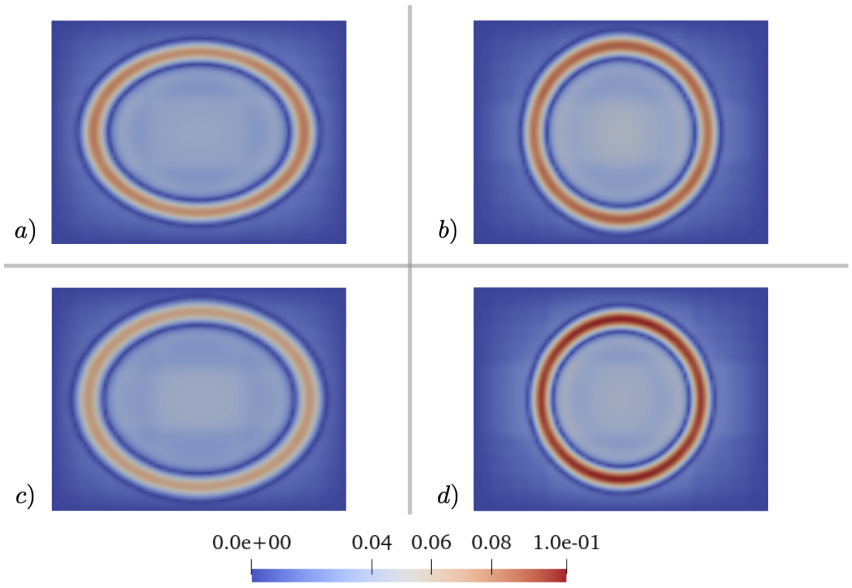

Figure 12. Comparison of physical effects over wave propagation at time $t = 0.3$. (a) Reference case: linear wave propagation without any pre-load. (b) Deformed geometry as for $\bar{\lambda}_1 = 1.2$, but no pre-load effect accounted in the problem. (c) Solution for $\bar{\lambda}_1 = 1.2$ with related material stiffness, while the geometric stiffness term is neglected ($\sigma_0 = 0$). (d)Solution for $\bar{\lambda}_1 = 1.2$ with related geometric stiffness, while the material stiffness term is neglected ($\zeta = 4$).

6 Conclusion

In conclusion, we have presented a stable, robust and efficient explicit scheme for the simulation of linear elastic wave propagation in nearly-incompressible solids. Furthermore, the scheme allows the approximation of solids with non-cartesian geometries subjected to large static deformations.

The efficiency of the scheme is based on the use of *damped Chebyshev polynomials*, applied here for the first time to treat dynamic problems with nearly-incompressible solids. This method, together with the space discretization strategy, guarantees a reduction of simulation time of at least a factor 2 with respect to the Leap-Frog method, second order convergence and preservation of energy. Finally, we have

753 presented the applicability of the scheme for wave propagation in non-linear solids
754 with large deformations.